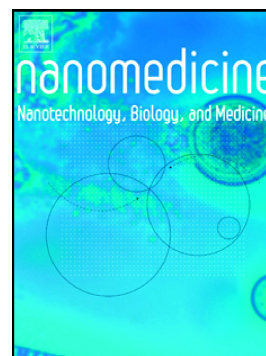


Journal Pre-proof

Melanin-based Nanomaterials: The promising Nanoplatfoms for
Cancer diagnosis and therapy

Zheng-Yuan Hong, Hong-Yan Feng, Li-Hong Bu



PII: S1549-9634(20)30065-4

DOI: <https://doi.org/10.1016/j.nano.2020.102211>

Reference: NANO 102211

To appear in: *Nanomedicine: Nanotechnology, Biology, and Medicine*

Revised date: 31 March 2020

Please cite this article as: Z.-Y. Hong, H.-Y. Feng and L.-H. Bu, Melanin-based Nanomaterials: The promising Nanoplatfoms for Cancer diagnosis and therapy, *Nanomedicine: Nanotechnology, Biology, and Medicine* (2020), <https://doi.org/10.1016/j.nano.2020.102211>

This is a PDF file of an article that has undergone enhancements after acceptance, such as the addition of a cover page and metadata, and formatting for readability, but it is not yet the definitive version of record. This version will undergo additional copyediting, typesetting and review before it is published in its final form, but we are providing this version to give early visibility of the article. Please note that, during the production process, errors may be discovered which could affect the content, and all legal disclaimers that apply to the journal pertain.

© 2020 Published by Elsevier.

Melanin-Based Nanomaterials: The Promising Nanoplatforms for Cancer Diagnosis and Therapy

Hong, Zheng-Yuan, Ph.D.^{1, †}; Feng, Hong-Yan, Ph.D.^{1, †}; Bu, Li-Hong, Ph.D.^{†, *}

[†] PET-CT/MRI Center, Molecular Imaging Center, Renmin Hospital of Wuhan University, Wuhan 430072, People's Republic of China

¹ The two authors contributed equally to this work.

* Address correspondence to bulihongs@whu.edu.cn.

Word count for abstract, manuscript; Number of references and figures

Word count of abstract: 142 words

Word count of manuscript: 11299 words

Number of references: 110

Number of figures: 10

Funding: This work was supported by the National Natural Science Foundation of China [grant numbers 81801840, 81871419, 81701735], the Fundamental Research Funds for the Central Universities [grant numbers 2042018kf0067], Natural Science Foundation of Hubei Province [grant numbers 2017CFB781], Chinese Society of Clinical Oncology Foundation [grant numbers Y-HR2016-44], Seed Project in Sino Foreign Joint Research Platform of Wuhan University [grant numbers 2309-413100006].

There is no commercial association in this paper, current and within the past five years.

Abstract

Melanin-based nanoplatforms are biocompatible nanomaterials with a variety of unique physicochemical properties such as strong photothermal conversion ability, excellent drug binding capacity, strong metal chelation capacity, high chemical reactivity

and versatile adhesion ability. These innate talents not only make melanin-based nanoplateforms be an inborn theranostic nanoagent for photoacoustic imaging-guided photothermal therapy of cancers, but also enable them to be conveniently transferred into cancer-targeting drug delivery systems and multimodality imaging nanoprobe. Due to the intriguing properties, melanin-based nanoplateforms have attracted much attention in investigations of cancer diagnosis and therapy. This review provides an overview of recent research advances in applications of melanin-based nanoplateforms in the fields of cancer diagnosis and therapy including cancer photothermal therapy, anticancer drug delivery, cancer-specific multimodal imaging and theranostics, etc. The remaining challenges and prospects of melanin-based nanoplateforms in biomedical applications are discussed at the end of this review.

Keywords melanin, polydopamine, cancer, imaging, therapy, theranostics

1. Introduction

Cancer is one of the main reasons of mortality worldwide, and it is estimated that about 21.6 million patients would be diagnosed with cancer diseases by the year of 2030.¹ To date, lots of efforts have been made to improve the efficiency of cancer diagnosis and therapy. Recently, the rapid development of nanomedicine offers an opportunity to provide innovative and precise cancer diagnostic or cancer therapy, which would facilitate improving the clinical performances with reduced adverse side effects.² In this respect, biocompatible, flexible and powerful nanoplateforms are highly desired for clinically potential cancer nanomedicine. Natural molecules in living organisms are promising alternatives and play crucial roles in development of biomedical nanoplateforms.

Melanins are a class of natural biopolymers widely distributed in many living organisms. They play important physiological roles in biological systems including thermoregulation, photoprotection, chelation, antioxidation, and some nervous system involvement.³⁻⁵ In the past decades, melanins were popularly used as a typical biomarker for diagnosis of melanoma and Parkinson diseases, and a series of melanin-targeted

molecular probes have been developed.⁶⁻¹⁰ Presently, inspired by their native photoacoustic property,¹¹ scientists have successfully transferred the biomarkers into contrast agents for photoacoustic imaging (PAI).^{12, 13} Because of their intrinsic chelating function, melanins were further developed into multimodality imaging nanoplatfoms by chelating $^{64}\text{Cu}^{2+}$ and Fe^{3+} for positron emission tomography (PET) and magnetic resonance imaging (MRI).¹⁴ Interestingly, on the basis of the finding that melanins have the capability of binding the drugs with aromatic structures through π - π interaction,¹⁵ melanin can be also used as a nanocarrier for drug delivery.¹⁶ By combining these properties together, melanin nanoparticles could be conveniently functioned as highly promising theranostic nanoplatfoms for potential clinical translation.

As endogenous molecules with the above attractive properties, melanins have been continuously applied in many ways. Generally, melanins have been classified into eumelanin and pheomelanin according to their different precursor molecule. Eumelanins are mostly biopolymers formed from phenolic compounds by polymerization via quinones,¹⁷ and is the mostly used melanin in biological and technological fields. However, there is no single well-defined structure for eumelanins due to their high-molecular weight polymeric chains or aggregates of oligomers.¹⁸⁻²⁰

Polydopamine (PDA) is a kind of synthetic materials produced by auto-oxidation of dopamine in mildly alkaline aqueous solutions. Because of the similar chemical structure as eumelanins, PDA is expected to possess the similar properties as eumelanins including NIR-responsive properties, chelation, and capability of drug binding. Hence, we here also classify PDA as melanin-based material. Inspired by the photoprotective function of eumelanins, Liu and colleagues have demonstrated the remarkable photothermal conversion ability of PDA, and transferred the PDA nanoparticles into photothermal therapeutic agents for in vivo cancer treatment.²¹ On the basis of this pioneering work, PDA was popularly used as a new generation of photothermal therapeutic nanoplatfom. Besides, the heat generated by photothermal conversion of PDA can also induce thermal expansion and generate ultrasonic waves, which is the basis for in vivo photoacoustic (PA) imaging. Furthermore, the native catechol and amino functional groups give PDA the ability of

chelating Fe^{3+} , Gd^{3+} , Mn^{2+} , $^{64}\text{Cu}^{2+}$ ions, and enable PDA to perform as MRI and PET agents for multimodality imaging.²²⁻²⁵ These unique properties make PDA become a promising candidate for clinically potential cancer nanomedicine, and PDA has been developed into a series of nanoplatforms for cancer therapy, imaging, and theranostic.

Within this review, we will summarize several applications of melanin-based nanoplatforms in cancer targeted therapy, imaging and theranostics (Figure 1), aiming to outline the recent developments in melanin-based nanoplatforms. It is expected that this review will provide a valuable reference for the rational design and application of melanin-based nanoplatforms in cancer diagnosis and therapy.

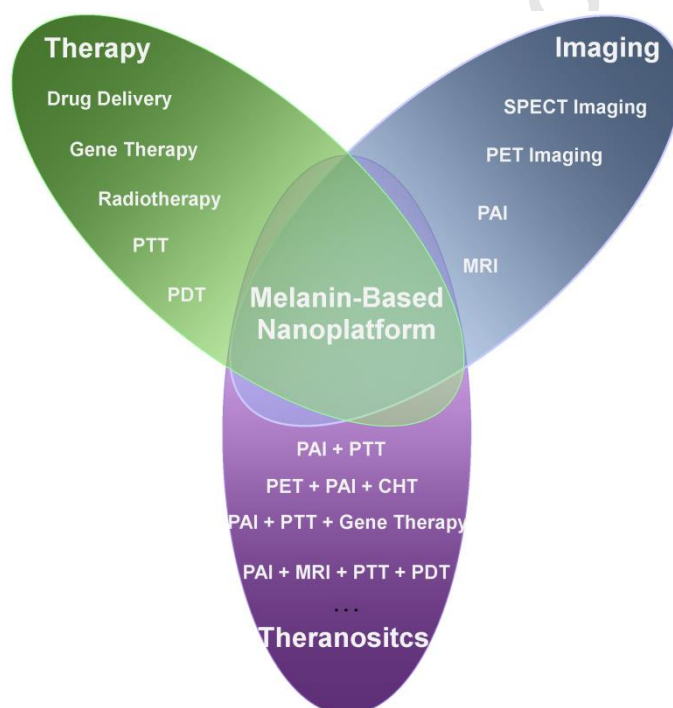


Figure 1 Schematic illustration of the applications of melanin-based nanoplatforms in cancer therapy, imaging and theranostics.

2. Synthesis and Physicochemical Properties of Melanin-Based Nanomaterials

2.1 Synthesis of Melanin and PDA

As mentioned above, eumelanin is the mostly used natural melanin-based materials in biotechnological fields. The biological pathway of eumelanin synthesis in epidermal melanocytes was described in Figure 2a.¹⁸ Tyrosine is oxidized to 3,4-dihydroxy-phenylalanine (DOPA) and then to DOPAquinone through

Tyrosinase-catalysis. The cyclization of DOPAquinone leads to the formation of dopachrome. Isomerization of dopachrome in two pathways gives two different monomers. Spontaneous isomerization of dopachrome with decarboxylation gives rise to the formation of 5,6-dihydroxyindole (DHI), whereas in the isomerization reaction with assistance of tyrosinase-related protein 2, the isomerization of dopachrome gives the product of 5,6-dihydroxyindole-2-carboxylic acid (DHICA). The following oxidative polymerization of monomers DHI and/or DHICA would lead to the deposition of eumelanin polymers. However, as aforementioned in Introduction, there is no single well-defined structure for natural melanins due to their high-molecular weight polymeric chains or aggregates of oligomers.¹⁸⁻²⁰ Most natural melanins are of large size, irregular shape, and insolubility in aqueous solution, thus needing necessary modification to adapt for biomedical applications. In the work reported by Fan et al.,¹⁴ water-soluble melanin-based nanoparticles with a ultrasmall size of 4.5 ± 0.5 nm were obtained by the procedure that dissolving pristine melanin granule into 0.1 N NaOH solution and then neutralized with assistance of sonication to reduce inter-chain aggregation. The obtained natural melanin-based nanoparticles exhibited water-solubility of 40 mg/mL and good stability, which could be attributed to the high negative surface potential of approximately -22.2 mV that blocked the aggregation of obtained nanoparticles via electrostatic repulsion.

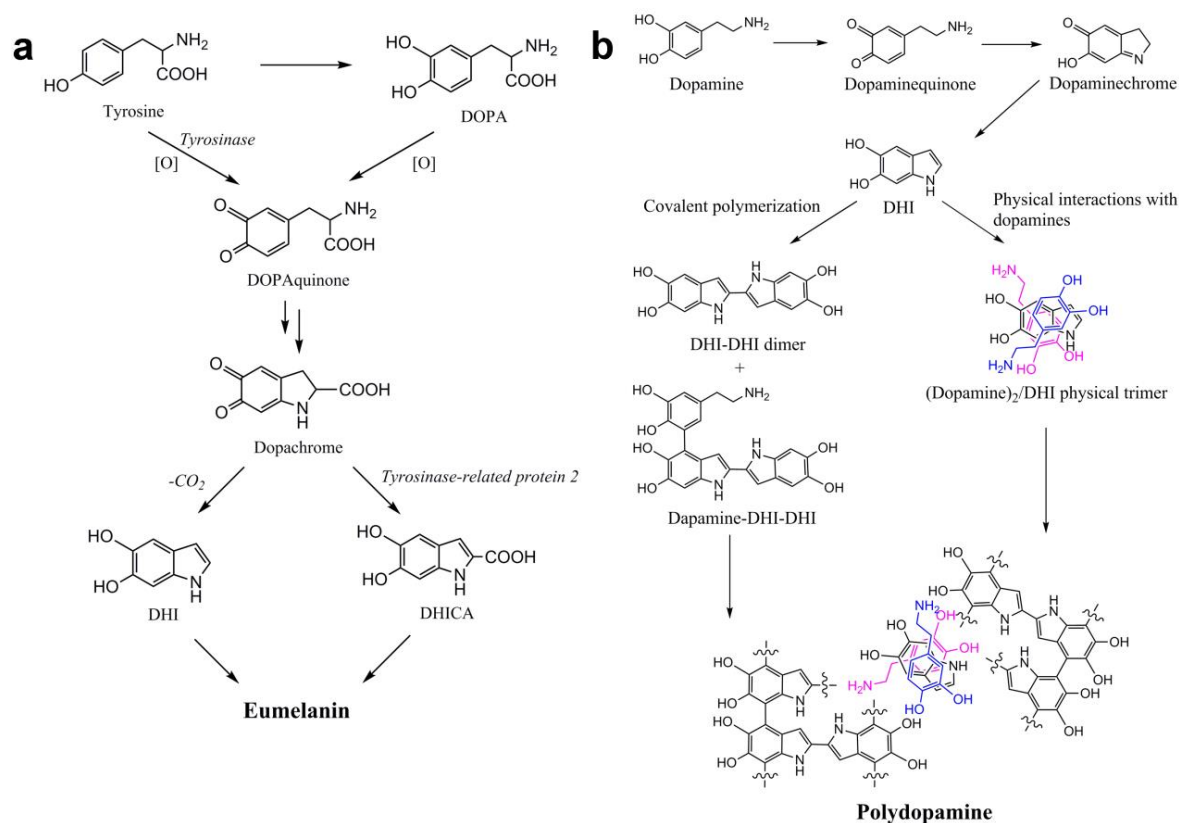


Figure 2 Schematic illustration of the synthesis processes of eumelanin (a) and PDA (b).^{18, 26}

PDA can be synthesized through the oxidative polymerization of dopamine, but it is still unclear about the molecular mechanism of dopamine polymerization. At present, it is widely accepted that dopamine is oxidized to quinones by the dissolved oxygen in solution, and the followed intramolecular cyclization of quinones leads to the formation of DHI (Figure 2b).²⁶ Then, two different pathways exist for DHI to construct PDA. Covalent oxidative polymerization of DHI and unpolymerized dopamine are able to form covalently bonded DHI dimers, dopamine-DHI-DHI trimeric conjugates and so on. Non-covalent self-assembly of DHI and unpolymerized dopamine is able to form (dopamine)₂/DHI physical trimer via the intermolecular interactions including H-bonding, T-shape interaction, and cation- π interaction.²⁶ The two pathways synergistically contribute to the formation of PDA. Thus, the complex compositions make it difficult to accurately define the chemical structure of PDA. Generally, PDA nanoparticles can be conveniently prepared through auto-oxidation of dopamine in solution, and solution with modestly high pH can promote the oxidation and self-polymerization of dopamine.²⁷ A widely used preparation method

was to stir dopamine in solution mix of ethanol, ammonia, and deionized water at room temperature for hours, and then harvesting the PDA nanoparticles through centrifugation.²¹

2.2 Physicochemical Properties

Melanin-based nanomaterials possess many attractive properties that are promising in cancer diagnosis and therapy. The absorption spectrum is broad-band monotonic, which makes melanin-based nanomaterials more like inorganic semiconductor material than organic chromophore. Absorption of the optical radiation energy is mostly subject to rapid nonradiative decay, such as being converted into heat. Some investigations illuminated the photothermal conversion with the principle of electron-phonon coupling,²⁸ which indicates the radiation energy excited electron to excited state and then was transferred to vibrational and rotational internal degrees of freedom of melanin or PDA molecules, and these states then rapidly nonradiatively relaxed.²⁸ In vivo, the heat generated by photothermal conversion can lead to a change in temperature of tissue, thus inducing thermal expansion which can results in the tissue volume change. In this case, pulsed optical radiation can induce frequently changes in tissue volume, which results in the generation of acoustic waves. Detecting the acoustic waves can enable the imaging of tissues. Hence, the photothermal conversion ability makes melanin-based nanomaterials become innate theranostic reagents for cancers.

Plenty of π -conjugated structures, amino, quinonyl and hydroxyl enable the melanin-based nanomaterials to bind a variety of drugs with aromatic structures such as doxorubicin (DOX) and sorafenib (SRF) through π - π stacking and/or hydrogen bond interaction. Thus, melanin-based nanomaterials have potential to be used as an alternative nanoplatform for drug delivery. As we know, atoms of N and O are potential sites for metal coordination. Large amounts of functional groups including catechol, hydroxyl, quinone, semiquinone, imine, amine, carboxyl containing in the melanin-based nanomaterials provide numerous sites for chelation of various metal ions such as iron ions and copper ions. The metal chelation capacity likely depends on the types of chelated metals and chelating conditions since the binding sites likely vary with type of chelated metals and change of

chelation conditions. For instance, it was concluded that the functional groups responsible for Fe^{3+} chelation were phenolic hydroxyl groups whereas that for Cu^{2+} were carboxylate and/or amine groups under pH 2-7 and hydroxyl(phenolic) groups under pH 7-11, respectively.^{5, 29} Metal chelation talent is able to confer specific capabilities on melanin-based nanomaterials such as chelating paramagnetic metals for MRI and so on.

Strong adhesion to a wide range of materials regardless of complex shape is an intriguing inherent talent of melanin-based materials.³⁰ Although the actual mechanism of adhesion remains elusive, one mechanism explanation indicated that the presence of catechol played a central role in adhesion. Catechol formed high-strength yet reversible coordination bonds with inorganic materials whereas oxidized catechol was able to form covalent bonds with organic materials.³¹ The adhesion ability was capable of conveniently conferring inborn talents of melanin-based materials on various materials. In addition to the adhesive ability, the catechol could be oxidized to quinone for cross-linking with amino- or thiol-terminated molecules via Michael addition or Schiff base reaction, and the amine and imine groups could enable the conjugation of melanin-based nanomaterials with carboxyl-containing molecules.³² Hence, these functional groups exposed on the surface of melanin-based nanomaterials are capable of covalently linking cancer biomarker targeting molecules such as antibodies and aptamers to improve the specificity for cancers.

3. Melanin-Based Nanoagents for Cancer Therapy

For cancer treatment, a therapy with high efficiency and reduced adverse side effects is of importance to cancer patients. Currently, the mostly used clinical therapies are surgery, chemotherapy (CHT) and radiotherapy. However, these conventional therapies have some adverse side effect issues including incidence of second cancers, toxicity and damage on normal tissues and immune system.^{33, 34} The recent strategies of cancer-targeted phototherapy and drug delivery provide the possibilities for precise localized cancer treatment, which facilitate to increase cancer therapy efficiency and reduce the adverse side effects. Melanin-based nanoplatfoms are promising alternatives for design and synthesis of cancer-targeted therapy nanoagents because of their excellent innate properties such as high

photothermal conversion efficiency, good biocompatibility, versatile adhesion, native drug binding capacity and high chemical reactivity.

3.1 Melanin-Based Nanoagents for Photothermal Therapy

The principle of photothermal therapy (PTT) is that the photothermal agents (PTA) can absorb radiant energy of light and convert it to thermal energy which can destroy cancer cells.³⁵ Compared to conventional therapies, PTT possesses several advantages such as simplified procedure, faster recovery and shorter hospital stay.³⁶ In an inspirational work, Liu and co-workers synthesized a novel dopamine-melanin colloidal nanosphere (CNS) with an average diameter of approximately 160 nm (Figure 3a) via oxidation and self-polymerization of dopamine.²¹ The size of CNS was tunable by changing the molar ratio between ammonia and dopamine in the synthesis. To adapt for potential practical applications, the dopamine-melanin CNS with relatively small size of 70 nm was used for in vivo cancer PTT experiments because of the slower clearance of small particles than that of large particles by phagocytes.³⁷ This synthetic CNS exhibits a broad optical absorption ranging from ultraviolet (UV) to NIR wavelengths (Figure 3b) and favorable stability in 10% blood serum solution more than 24 h, indicating good potential for in vivo use. In vitro photothermal conversion experiments revealed that the temperature of 200 $\mu\text{g/mL}$ dopamine-melanin CNS solution could be increased by 33.6 $^{\circ}\text{C}$ after irradiation of 808 nm laser at 2 W/cm^2 for 500 s (Figure 3c and 3d). This was likely to be sufficient for killing cancer cells since temperature of human body was about 36 $^{\circ}\text{C}$ and cancer cells could not live at 50 $^{\circ}\text{C}$ for more than 6 min. Then, the photothermal conversion efficiency calculation was performed on the basis of the formula: $\text{Efficiency} = (hA\Delta T_{\text{max}} - Q_s) / [I(1 - 10^{-A_{\lambda}})]$, where h was heat transfer coefficient, A was surface area of container, ΔT_{max} was temperature change of nanoparticle solution at the maximum steady-state temperature, Q_s was the heat associated with the light absorbance of solvent, I was the laser power, A_{λ} was absorbance of nanoparticles at 808 nm.²¹ The calculation results showed that dopamine-melanin CNS possessed a photothermal conversion efficiency of 40%, which was relatively higher than that of Au nanorods (22%). This was attributed to the reason that

the morphology change of Au nanorods induced by local heating resulted in their significant loss in NIR absorbance whereas no similar phenomena observed for dopamine-melanin CNS. PTT efficacy was assessed by in vivo experiments. After intratumorally injecting the dopamine-melanin CNS into 4T1 tumor bearing mice, the tumors were exposed to an laser of 808 nm at 2 W/cm^2 for 5 min (Figure 3e), and results showed that most of tumor tissues were necrotic and suppression of tumor regrowth was achieved in 10 days. Biodistribution investigation results suggested that dopamine-melanin CNS mostly accumulated in spleen and liver of 4T1 tumor-bearing mice at 24 h after intravenous injection (Figure 3f). Importantly, the mice could remain healthy more than 1 month with little adverse effects in tissues detected. These properties make melanin-based materials become promising building blocks for rational design of PTA.

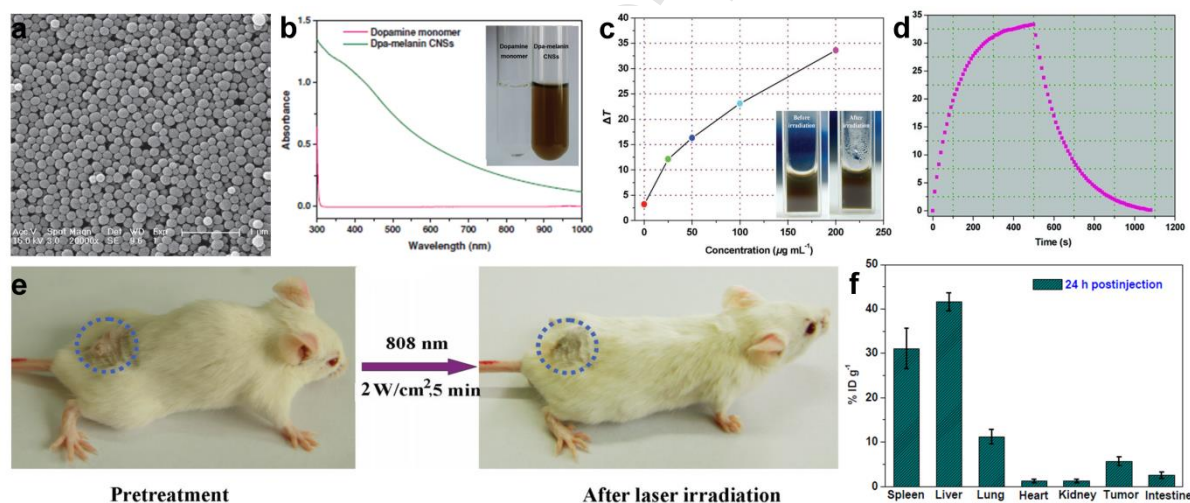


Figure 3 a) Scanning electron microscope image of dopamine-melanin CNS. b) UV-vis absorption spectrum of dopamine-melanin CNS and dopamine monomers. c) Temperature change over a period of 500 s versus the concentration of dopamine-melanin CNS. The inset exhibits dopamine-melanin CNS dispersion in water before and after laser irradiation. d) The photothermal response of the dopamine-melanin CNSs aqueous solution ($200 \mu\text{g/mL}$) upon the irradiation of 808 nm laser at 2 W/cm^2 for 500 s and then the laser was shut off. e) Photographs of a 4T1 tumor-bearing mice before and after PTT. f) Biodistribution of the intravenously injected dopamine-melanin CNS in 4T1-tumor bearing mice at 24 h post-injection.²¹

From then on, a series of melanin-based PTAs have been developed for cancer PTT research, and natural melanin nanomaterials were promising alternatives. Chu et al. extracted black sesame melanin (BSM) from black sesame seed skins under alkaline conditions to prepare natural melanin-based nanoparticles for in vivo cancer PTT.³⁸ FT-IR and ¹H NMR spectra characterization described that the BSM should be consisted of aromatic rings containing multiple functional groups including hydroxyl, carboxyl, methyl and so on. Interestingly, Raman spectrum indicated that BSM nanoparticles should be a grapheme-like two dimensional nanomaterial. Then, BSM nanoparticles were encapsulated into liposome to improve their solubility in neutral solution, and the size of liposome-BSM composites was around 150 nm. Photothermal conversion of the nanoscale composites in vivo showed that 70 μ L composites containing 5 mg/mL BSM were able to increase the tumor temperature rapidly to 42.9 $^{\circ}$ C in 3 min and to 45.5 $^{\circ}$ C in 20 min under irradiation of 808 nm laser. The photothermal conversion capacity was capable of significantly inhibiting the growth of Eca-109 tumor in mice after intratumoral injection of liposome-BSM composites. In another work, Kim and colleagues mixed 1 mg natural melanin with 3 mL of 20% (w/v) poloxamer407 solution to prepare Pol-Mel mixture for in vivo cancer PTT without any precipitation.³⁹ This Pol-Mel mixture could be localized at the injection site by sol-gel transition at body temperature to avoid unnecessary distribution to other tissues. Intratumoral injection of the mixture enabled the temperature of CT26 tumor tissue in mice to increase to 55 $^{\circ}$ C after local irradiation of 808 nm laser at 1.5 W/cm² for 3 min, which was able to inhibit the CT26 tumor growth.

Besides the natural melanin-based PTAs, more and more synthetic PDA based nanoplatfoms were used as PTA for cancer therapy.⁴⁰⁻⁴² For instance, Li and co-workers have synthesized dopamine carbon nanodots (DA CNDs) with diameter of 23 nm via a facile hydrothermal method without assistance of passivating agents.⁴⁰ The DA CNDs exhibited a photothermal conversion efficiency of 35%, which was higher than that of Au nanorods. In vitro experimental results indicated that 50 μ g/mL DA CNDs were capable of killing a majority of Hella cells after irradiation of 808 nm laser at 1.5 W/cm² for 5 min. Ding et al. have used two different lipid nanotubes (LNTs) as templates for selectively

fabricating helically coiled and linear PDA nanotubes.⁴¹ Compared to linear PDA-LNT, coiled PDA-LNT have advantages such as higher light absorbance efficiency and higher photothermal conversion efficiency.

In addition to be the building block of melanin-based PTA nanoparticles, PDA was also widely used to improve PTT efficacy of the PTAs that prepared with other materials, such as noble metals and carbon-based materials. Assembly of spherical gold nanoparticles (GNPs) into superparticles was able to shift the localized surface plasmon resonance (LSPR) to NIR region because of plasma coupling effect resulted from the short distance among GNPs, thus enhancing the photothermal effects of gold nanoparticles.^{43,44} Hence, Tian et al. coated GNPs with PDA to utilize the photothermal conversion capacity and dopamine chemistry of PDA to prepare gold hollow superparticles (GHSPs) with enhanced photothermal effect.⁴⁵ PDA-capped GNPs (PGPs) were synthesized via the self-polymerization of dopamine on the surface of GNPs with the assistance of a Tris-Cl buffer under alkaline condition. Comparison between UV-vis spectrum of PGPs and GNPs suggested PDA-modification enhanced the absorbance of gold particles in NIR region due to the light harvest ability of PDA. Multi-amino poly(ethylene imine) (PEI) crosslinked PGPs to obtain GHSPs via the reaction between amine and PDA. Furthermore, methoxy-poly(ethylene glycol) amine (mPEG-NH₂) was modified on the GHSPs with a similar way to stabilize the structures of superparticles. The obtained GHSPs had a much stronger absorbance in the NIR region than PGPs and dopamine-melanin CNS, thereby having potential to be used for in vivo cancer PTT. The photothermal conversion efficiency of GHSPs was 38%, which was much higher than that of PGPs (15%) and slightly lower than that of dopamine-melanin CNS. After intratumoral injection of 1.0 mg/kg GHSPs into MCF-7 tumor bearing mice, the photothermal conversion capacity of GHSPs could rapidly increase the tumor temperature to 60 °C when mice exposed to the irradiation of 808 nm laser at 2 W/cm² for 5 min. This was enough to kill cancer cells and showed good potential of GHSPs in cancer PTT. The GHSPs leaked into circulation could be taken up by liver and spleen. In another work, Li et al. coated branched Au-Ag nanoparticles with PDA through spontaneous polymerization of dopamine on the surface to improve the structural stability,

biocompatibility and photothermal conversion efficiency.⁴⁶ Interestingly, increase of PDA shell thickness was able to increase the photothermal conversion efficiency of Au-Ag@PDA nanoparticles. When the PDA shell thickness was 10 nm, the photothermal conversion efficiency of Au-Ag@PDA nanoparticles was up to 61.4%, which was higher than that of nude Au-Ag nanoparticles (55.8%), Au nanorods (22%), and dopamine-melanin CNS (40%). For carbon-based materials, chemically modified graphene oxide (GO) have the potential to be a multifunctional agent in PTT. However, the much less NIR absorption than other nanomaterials limited the use of GO in PTT. Reduced GO (rGO) may be a better alternative in PTT. Hence, Yu et al. took use of dopamine to reduce GO to prepare PDA/rGO composites for in vivo PTT research.⁴⁷ In this process, spontaneous oxidative polymerization of dopamine simultaneously accompanied with reduction of GO, thus finally achieving the coating of PDA on the surface of rGO. UV-vis absorption characterization showed that PDA modification significantly improved the optical absorption of GO in NIR region. Then, PDA/rGO nanocomposites were further functionalized with antiarrhythmic peptide 10 (AAP10) peptide via Michael addition and/or Schiff base reaction. AAP10 peptide could elevate activity of Cx43 in cancer cells to suppress carcinogen-induced neoplastic transformation, thus further improving the cancer therapeutic efficiency. Atomic force microscopy characterization suggested that the thickness of PDA/rGO was 3.5 nm, 2.4 nm thicker than monolayered GO, and AAP10 peptide functionalization induced little thickness increase. Photothermal conversion efficiency of AAP10-PDA/rGO was 49.1%, which was much higher than that of GO (25.4%) and rGO (41%).^{48, 49} After intratumoral injection into 4T1 breast-tumor bearing mice, both of AAP10-PDA/rGO and PDA/rGO could increase the temperature of tumor to approximately 52 °C when the tumor bearing mice were irradiated by 1.5 W/cm² 808 nm laser for 5 min, which was enough to kill cancer cells. Moreover, the presence of AAP10 peptide strongly suppressed the recurrence of 4T1 breast tumor after PTT, thus further improving the cancer therapeutic efficiency of PDA/rGO nanocomposites.

3.2 Melanin-Based Nanoagents for Combination Therapy

Actually, PTT has inherent limitations such as incomplete destroy of cancer tissues since the light absorption and scattering in biological tissues and uneven distribution of hyperthermia and intermittent NIR radiation. Combination of PTT and other therapy methods would offer an opportunity to improve the cancer therapeutic effects and reduce the adverse side effects. Fortunately, melanin-based nanoplateforms exhibited not only the photothermal conversion ability, but also strong drug adsorption ability and high chemical reactivity because of their abundant aromatic structures and chemically active groups, indicating melanin-based materials have potential to be transferred into drug delivery system (DDS).⁵⁰⁻⁵³

For example, Cui et al. have conjugated DOX to thiolated poly(methacrylic acid) with a pH-cleavable hydrazone bond, and then immobilized the conjugates to PDA capsules under alkaline condition via Michael addition between thiol and PDA.⁵⁰ Hence, this was a pH-dependent drug release DDS, and UV-vis absorbance characterization suggested that each 300 nm PDA capsule loaded with about 6.45×10^{-16} g DOX. In vitro drug release experimental results showed that this DDS was able to release 85% DOX at an acidic pH of 5.0 in 12 h whereas less than 20% drug was released at physiological pH 7.4 in the same duration. In another work, Zhu et al. utilized PDA nanoparticles as DDS to carry an anticancer drug cisplatin through the interactions between platinum and catechol groups on PDA (PEG-PDA-CP).⁵⁴ The amount of cisplatin in PEG-PDA-CP was 20% (w/w), and the drug release was also pH-dependent since the protonation of oxygen groups in acidic environment could lead to decomposition of PDA-drug composites. When the temperature was 37 °C, PEG-PDA-CP could release 45% drug in 36 h and 55% drug in 72 h at pH 6.0 whereas 33.3% drug was released in 72 h at pH 7.4. These pH-triggered drug-release DDS could provide an alternative way to enhance the anti-cancer drug release in the acidic microenvironment of tumor sites.

The promising drug delivery capability and inherent photothermal conversion ability enable melanin-based nanoplateforms to achieve combination of PTT and CHT for cancer treatments.⁵⁵ In an intriguing work, Wang et al. used PDA nanoparticles as a cross-linker to cross-link 20 kDa 4-arm-poly(ethylene glycol) (4-arm-PEG-SH) to prepare PDA knotted

PEG hydrogel for loading of anticancer drug 7-ethyl-10-hydroxycamptothecin (SN38) (PDA-SN38/PEG hydrogel).⁵⁶ Briefly, spherical PDA nanoparticles with diameter of 78 nm were synthesized according to the typical method based on the oxidative polymerization of dopamine under alkaline condition. Then, the PDA nanoparticles primarily loaded with SN38 via π - π stacking and followed by cross-linking with 4-arm-PEG-SH via dopamine chemistry to fabricate PDA-SN38/PEG hydrogel. Drug loading significantly increased the hydrodynamic size of PDA nanoparticles by 17 nm and slightly changed zeta potential of PDA nanoparticles. UV-vis absorbance revealed that the drug loading ratio of SN38 on PDA nanoparticles was variable and could reach to 11.8% when 6 mg SN38 mixed with 4 mL 1.9 mg/mL PDA nanoparticles, in which the drug loading ratio was calculated by the formula: drug loading ratio = drug mass \times 100% / (drug mass + nanoparticles mass). NIR laser irradiation enabled effective release of SN38 from PDA-SN38/PEG hydrogel whereas minimal SN38 released from nonirradiated hydrogel under physiological conditions because of the strong π - π stacking interactions between chemical drugs and PDA. NIR irradiation could be also converted into heat by PDA for cancer PTT, thereby achieving the synergistic cancer therapeutic effects of PTT and CHT, which was exhibited by in vivo experimental results. Upon the irradiation of 808 nm laser at 0.58 W/cm² for 5 min, intratumorally administered PDA-SN38/PEG hydrogel increased PC-9 tumor temperature by 9 °C to 44 °C, which was enough for killing cancer cells. NIR irradiation every 2 days enabled the continuous release of drug for cancer CHT, thus successfully suppressing the tumor growth. Importantly, the hydrogel caused no significant foreign-body reaction in vivo in a long time, exhibiting an excellent biocompatibility. In another work of this group, they used PEG-modified PDA nanoparticles (PDA-PEG) to load with anticancer drugs DOX and SN38 for investigation of the drug release behaviors triggered by multiple stimuli including NIR irradiation, pH and reactive oxygen species (ROS).⁵⁷ Spherical PDA nanoparticles with diameter of 78 nm were synthesized according to the abovementioned typical method, and then were modified with PEG to improve their biocompatibility (Figure 4a and 4b). Photothermal conversion ability was able to increase solution temperature by 26.4 °C when 200 μ g/mL PDA-PEG was irradiated by 808 nm laser at 3.6 W/cm² for 10 min while

that determined from water was 4.3 °C (Figure 4d). PDA-PEG was capable of loading with DOX and SN38 via π - π stacking and/or hydrogen bond interaction (Figure 4c and 4f), and the weight ratio of drug-loading was up to 33.0% for DOX and 10.8% for SN38. Then, drug release behaviors triggered by multiple stimuli has been investigated as follows (Figure 4e). NIR irradiation at 3.6 W/cm² for 30 min enabled the drug-loaded PDA-PEG to release 23.1% DOX and 58.6% SN38, which was much higher than that without NIR irradiation (Figure 4g). In an acidic condition of pH=5.0, drug-loaded PDA could release 14.5% DOX and 25.3% SN38 in 12 h (Figure 4h), which should be attributed to the reason that protonation of amine groups on the PDA and/or drug molecules partially destroy the π - π interactions between PDA and drugs. Moreover, the drug-loaded PDA nanoparticles could release 20.3% DOX and 36.3% SN38 after 12 h incubation with 20 mM H₂O₂ (Figure 4h). This was because H₂O₂ oxidized the polyphenol groups in the PDA and broke the hydrogen bonding interactions between PDA and drugs. Hence, the acidic microenvironment and ROS in cancer tissues would facilitate the anticancer drug release. Then, PDA-PEG/DOX nanoparticles were intratumorally injected into the PC-9 tumor-bearing mice to study their therapeutic effects in vivo. Results suggested that tumor suppression has been achieved by PTT-CHT synergistic effects, in which PTT played a major role. In the therapeutic period, there was no detectable pathological change in main organs caused by PDA-PEG/DOX nanoparticles.

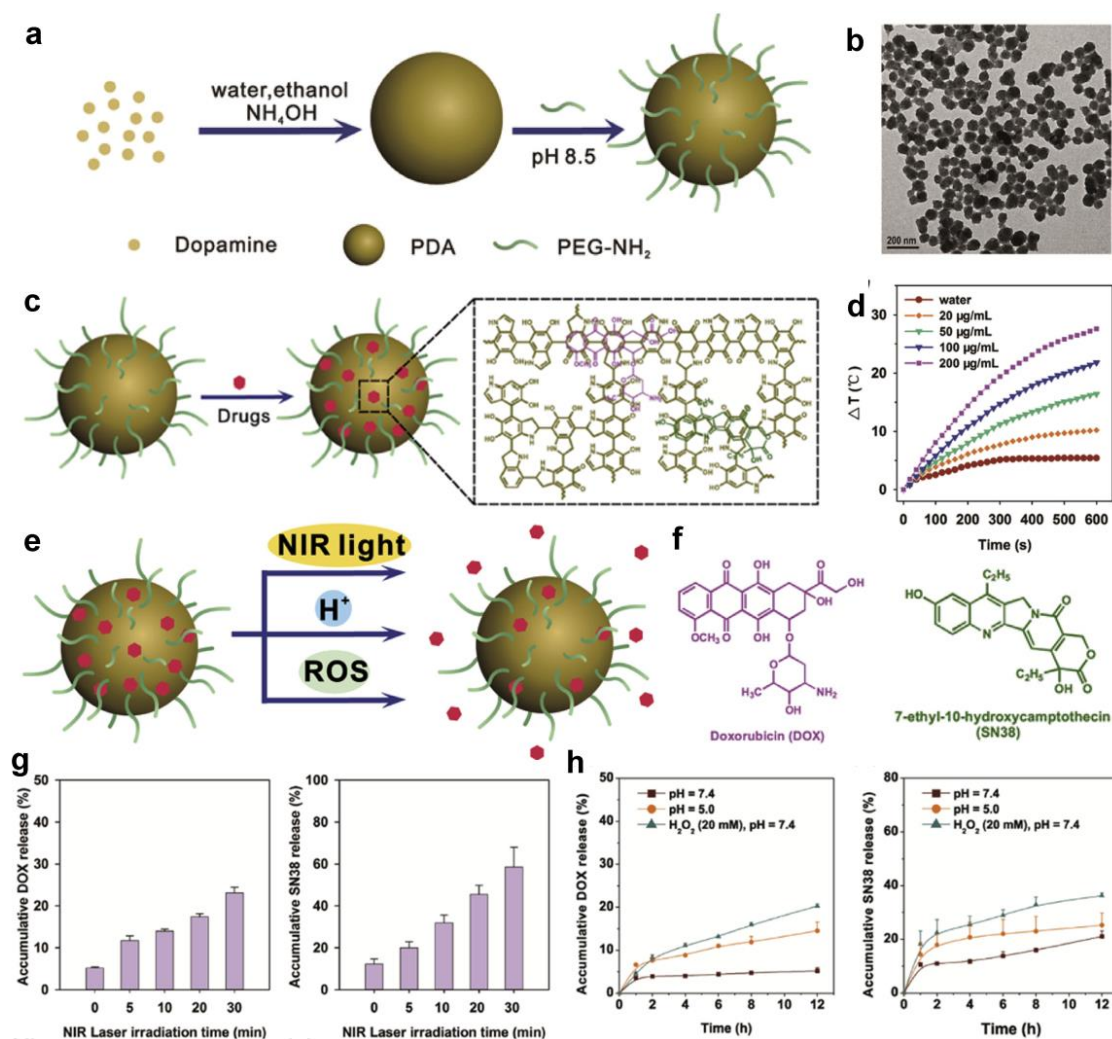


Figure 4 a) Synthesis route of PEG-modified PDA nanoparticles. b) TEM image of PEG-modified PDA nanoparticles. Scale bar represents 200 nm. c) Schematic illustration of drug-binding on PDA. d) Temperature changes of PDA solution at different concentrations upon the irradiation of NIR laser at 3.6 W/cm². e) Schematic illustration of multiple stimuli-responsive drug release of PDA nanoparticles. f) Chemical structures of DOX and SN38. g) Percentages of the drug release from DOX-loaded and SN38-loaded PDA nanoparticles triggered by NIR irradiation at different time. h) The drug release from DOX-loaded and SN38-loaded PDA nanoparticles triggered by acidic pH and ROS at different time.⁵⁷

Functionalization of melanin-based nanoparticles with some specific functional groups would further enhance the PTT-CHT synergistic effects on cancer cells. For example, it is well-known that cancer cells can develop drug resistance, and one main reason is that drug can efflux from cancer cells by ATP-binding cassette transporters such as P-glycoprotein.⁵⁸

The D- α -tocopheryl polyethylene glycol 1000 succinate (TPGS) was capable of targeting mitochondrial organelles and suppressing ATP-production activity of mitochondria,^{59, 60} thus having potential to reduce the effluxion of anti-cancer drugs from cancer cells. Xing et al. have used mesoporous PDA nanoparticles (MPDA) to bind DOX and functionalized the surface of MPDA with TPGS for combined PTT-CHT of multiple drug resistance cancer cells.⁶¹ The MPDA exhibited a drug loading capacity of 2 mg/mg because of their high specific surface area and hollow cavity. TPGS was tightly integrated with MPDA via the π - π stacking and hydrophobic interaction between its hydrophobic vitamin-E tail and MPDA. The DOX release of MPDA could be achieved by multiple stimuli including acidic pH, glutathione, and NIR irradiation. These stimuli could increase the release degree of drug by 15%, 25%, and 50%, respectively. Expectably, the presence of TPGS was able to promote cytotoxicity of DOX to P-glycoprotein over-expressing MCF-7 cells in the in vitro experiments. Integration of abovementioned matters may have potential to enhance therapeutic effects of anticancer drugs on the tumors with drug resistance.

In addition to the pure melanin-based nanoparticles used for combination therapy, melanin-based materials are also widely used for functionalizing the surface of the inorganic or polymer nanoplatfoms that with specific properties to confer the photothermal conversion ability and drug loading capacity on these nanoplatfoms to achieve controlled or enhanced synergistic PTT-CHT of cancers.⁶²⁻⁶⁸ As mentioned above, dopamine is able to reduce GO to prepare PDA/rGO composites under alkaline condition. Importantly, the PDA functionalization can not only enhance the photothermal effects of GO materials, but also confer chemical reactivity and drug loading capacity on this composite. Wang et al. utilized these properties to integrate PDA/rGO composites, gold nanostars (GNS), and DOX together for synergistic PTT-CHT of 4T1 breast cancer (Figure 5a).⁶⁹ In this work, GNS was loaded on the PDA/nanosized reduced GO (PDA/NRGO) composites via Au-catechol interaction to increase the absorbance in NIR region of PDA/NRGO (Figure 5b).^{70, 71} Then, the PDA/NRGO-GNS composites were further modified with thiolated PEG5k through the formation of Au-S and Michael addition with PDA to improve the colloidal stability of PDA/NRGO, and subsequently loaded with anticancer drug DOX via π - π

stacking and hydrophobic interactions to fabricate an integrated nanoplatform (NRGO-GNS@DOX) for in vivo cancer therapy. Due to the large surface of PDA/NRGO, NRGO-GNS@DOX achieved a DOX loading ratio of 67% when the mass ratio of NRGO-GNS to DOX was 0.45. Subsequently, the photothermal conversion ability and DOX release behaviors were determined in vitro. Loading GNS could increase the temperature elevation by 5 °C to about 23 °C when the particles were irradiated by 655 nm laser at 4.0 W/cm² for 90 s (Figure 5c). The integrated nanoplatform also exhibited a multiple stimuli drug release behavior such as pH- and/or hyperthermia-triggered DOX release. In this work, NRGO-GNS@DOX was able to release over 70% DOX at pH 5.4 in 24 h, which was higher than the DOX release amount at neutral pH (Figure 5d). Moreover, laser irradiation could accelerate the release of DOX, and NRGO-GNS@DOX released over 80% DOX in 9 h with the irradiation of 655 nm laser at 1.6 W/cm² at indicated time points (Figure 5d). To study the therapeutic effects in vivo, this integrated nanoplatform was intratumorally injected into 4T1 breast tumor models for further research. When exposed to a 655 laser at 6.0 W/cm² for more than 60 s, NRGO-GNS@DOX could achieve the tumor temperature elevation of 55 °C, thus being able to kill cancer cells by hyperthermia effects. Furthermore, the DOX released from NRGO-GNS@DOX would cause apoptosis of cancer cells, thus further enhancing the tumor growth suppression. (Figure 5e and 5f).

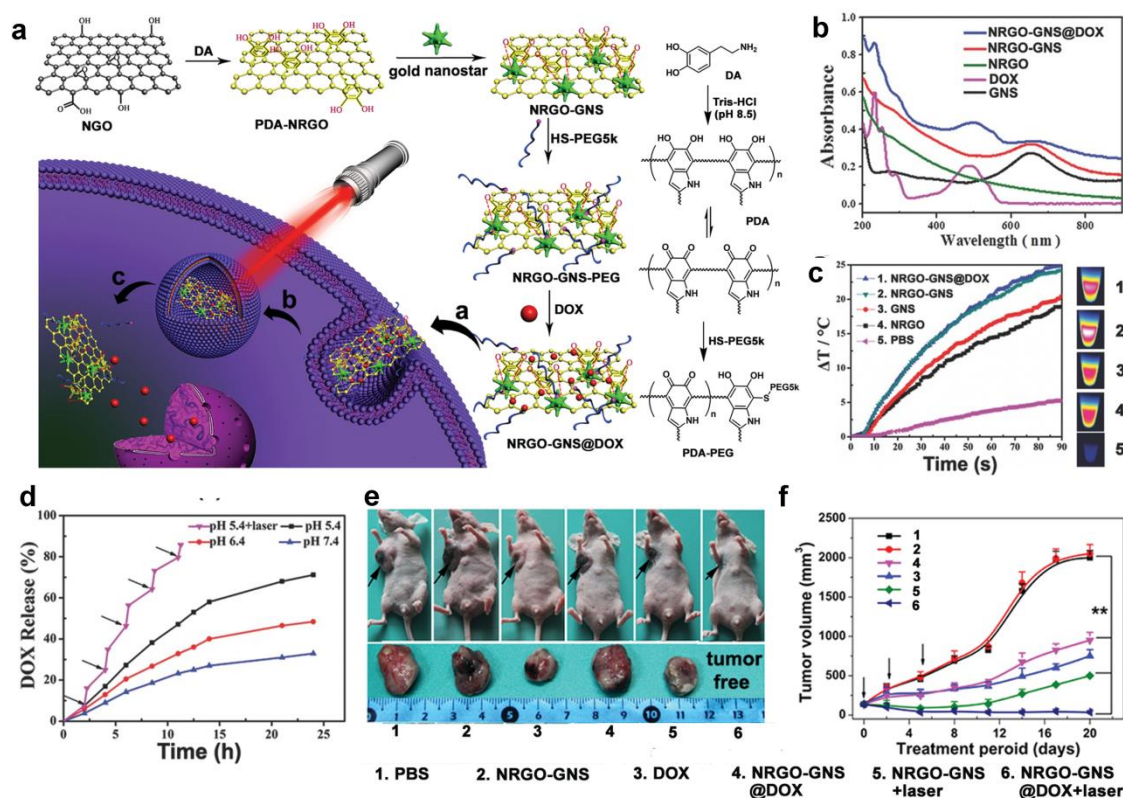


Figure 5 a) Schematic illustration for the construction of NRGO-GNS@DOX nanoplatform for synergistic PTT-CHT of breast cancer. b) UV-vis-NIR spectra of indicated samples. c) Temperature changes of indicated samples at different time upon the irradiation of 655 nm laser at 4.0 W/cm². d) DOX release profiles of the NRGO-GNS@DOX nanoparticles treated with indicated conditions. e) Photographs of the 4T1 tumor-bearing mice and the tumor tissue that taken out at the 20th day post treatment. f) Volume changes of tumor tissues during the therapeutic period ($n = 6$, $** p < 0.01$).⁶⁹

Besides PTT and drug loading, melanin-based materials were also applied to thermo-responsive drug release because of their good photothermal conversion ability. Ding et al. constructed a core-shell drug delivery nanosystem by use of the thermo-sensitive amphiphilic co-polymer P(MEO₂MA-co-OEGMA-co-DMAEMA)-b-PLGA for drug loading.⁷² This nanosystem encapsulated DOX and paclitaxel (TAX) in the hydrophilic core and hydrophobic layer, respectively. Then, siRNA against survivin was electrostatically adsorbed on the surface of nanosystem. However, over 30% of the loaded drugs would be initially burst released from the nanosystem in 8 h. Thus, the surface of this nanosystem was further coated with PDA to simultaneously prevent drugs from initial burst release and

confer the photothermal conversion ability on this nanosystem. This nanosystem, namely NP-DTS-PDA, could achieve a drug loading ratio of 9.81%. When irradiated by 808 nm laser at 1 W/cm^2 for 5 min, the hyperthermia generated by PDA was able to increase temperature from 29.8 to 56.7 °C, which was sufficient to induce the NP-DTS-PDA collapse and instant anticancer drug release. In vivo study suggested that the NP-DTS-PDA could passively accumulate in the tumor site in 24 h after intravenously injection due to the enhanced permeability and retention (EPR) effects. Localized laser irradiation for 5 min increased tumor temperature to 59.6 °C, which enabled killing cancer cells by hyperthermia and triggering drug release for tumor growth suppression. The thermo-responsive nanosystem integrated PTT, CHT, and gene therapy together, and induced effective cancer therapy with unapparent effects on main organs of tumor-bearing model.

4. Melanin-Based Nanoprobes for in vivo Cancer Imaging

Cancer diseases are one leading cause of mortality worldwide. Early diagnosis of cancer is of vital importance to the treatment outcome of patients. Furthermore, precise detection and identification of cancers are capable of monitoring the disease progression and relevant biological processes. Highly efficient diagnostic or imaging agents are capable of labeling the specific biomolecules of cancers and localizing the precise positions of tumor sites, thereby providing effective early diagnosis and therapeutic monitoring for precise cancer therapy.² Melanin-based materials are desirable building blocks for constructing cancer diagnostic or imaging agents because of their outstanding properties such as intrinsic photoacoustic property, good biocompatibility, high chemical reactivity, and excellent flexibility. These inherent properties enable melanin-based nanoplateforms to combine cancer recognition groups and multiple signal atoms and/or molecules together to construct nanoprobes with cancer specificity and multimodality imaging capacity. In this section, we introduced some melanin-based imaging nanoprobes for detection of cancers.

4.1 Melanin-Based Nanoprobes for Photoacoustic Imaging

In biomedical imaging, as abovementioned, generation of photoacoustic waves is attributed to the thermal expansion of tissues caused by photothermal effects.² The native photothermal conversion ability enables melanin-based materials to induce photoacoustic waves for PAI of in vivo cancers under NIR pulse laser irradiation.^{73,74} For example, Ju et al. introduced hydrolysis-susceptible citraconic amide on the surface of PDA nanoparticles to enable the nanoparticles aggregating under mildly acidic conditions to achieve an enhancement of photoacoustic signal, which has potential to be used in imaging of cancer tissues because of their acidic microenvironments.⁷⁵ In this work, spherical PDA nanoparticles with a diameter of 130 nm were synthesized via the spontaneous oxidative polymerization of dopamine under alkaline conditions. Subsequently, ethylenediamine was modified on the surface of the PDA nanoparticles through Schiff base and/or Michael addition reaction, and further linked with citraconic anhydride through the amide bonds formation, thus obtaining the citraconic amide modified PDA nanoparticles. These modifications were ascertained by measuring the changes in surface charge and FT-IR spectra. In the mildly acidic condition, hydrolysis reaction of citraconic amide made PDA nanoparticles exhibit both positive and negative surface charges, thus inducing the PDA nanoparticle aggregation through electrostatic interaction. The acidic pH-induced physical aggregation resulted in 8.1-fold increase of photoacoustic signal intensity in comparison with the PDA nanoparticles in neutral conditions after 90 min. This phenomenon was attributed to the reason that aggregation of PDA nanoparticles may induce the overlap of thermal fields and hence capable to increase the rate of the thermal flux and the photoacoustic signal intensity.⁷⁶ The photoacoustic signal amplification capability also worked in vivo. Results suggested that the photoacoustic signal intensity of tumor site in the B16 melanoma model was 2.4-fold higher than that of control at 2 h post-injection.

To date, efforts also have been made to obtain endogenous melanin-based photoacoustic nanoprobes. In a recent intriguing work, an *E. coli* bacterial strain was engineered to produce biopolymer-melanin loaded bacterial outer membrane vesicles (OMV^{Mel}) for contrast enhancement in PAI (Figure 6a).⁷⁷ In this work, a less endotoxic *E. coli* bacterial strain obtained via *msbB* gene inactivation was engineered to overexpress

tyrosinase for production of melanin, which was then encapsulated into OMV to give OMV^{Mel}. Analysis of TEM and hydrodynamic size showed that most of the bacteria-derived OMV^{Mel} were in the range of 20-100 nm (Figure 6b) with a circular and bilayer morphology (Figure 6d). OMV^{Mel} had a broad absorption spectrum as pure melanin (Figure 6c), and also possessed the photothermal conversion capability. In vitro experimental results indicated that OMV^{Mel} exhibited a photothermal conversion efficiency of 18.65%, which was able to increase the solution temperature by >10 °C from room temperature under the irradiation of 750 nm laser at 0.65 W/cm² for only 2 min (Figure 6e). The photothermal conversion of OMV^{Mel} could give relatively much stronger photoacoustic signal than wild type OMV (OMV^{WT}). Subsequently, OMV^{Mel} was injected into 4T1 tumor model via tail vein for in vivo PAI. As shown in Figure 6g and 6h, OMV^{Mel} could time-dependently accumulate in the 4T1 tumor tissues after injection. A favorable PAI of tumor sites could be achieved at 3 h after injection, and the photoacoustic signal was still evident at 24 h after injection. Moreover, the PAI revealed that OMV^{Mel} also circulated and distributed in other organs, especially liver and kidney. Also, the photothermal conversion capability of OMV^{Mel} enabled cancer PTT in vivo, and this work has compared the PTT efficacy of OMV^{Mel} on the 4T1 tumor bearing mice that received intravenously or intratumorally. After being exposed to 800 nm laser at 1.5W/cm² for 6 min at 3 h after injection, the tumor site temperature of intratumorally treated mice could reach to 56 °C which was higher than the 47 °C of intravenously treated mice (Figure 6f). Hence, intratumoral administration of OMV^{Mel} exhibited a better therapeutic effect on 4T1 tumor than intravenously administration: the former was capable of inhibiting cancer growth in 8 days while the latter could reduce the tumor growth by approximately 43% (Figure 6i). In this case, the entirely biological synthesized OMV^{Mel} had potential to become a biocompatible theranostic nanoplatform for cancer diagnosis and therapy.

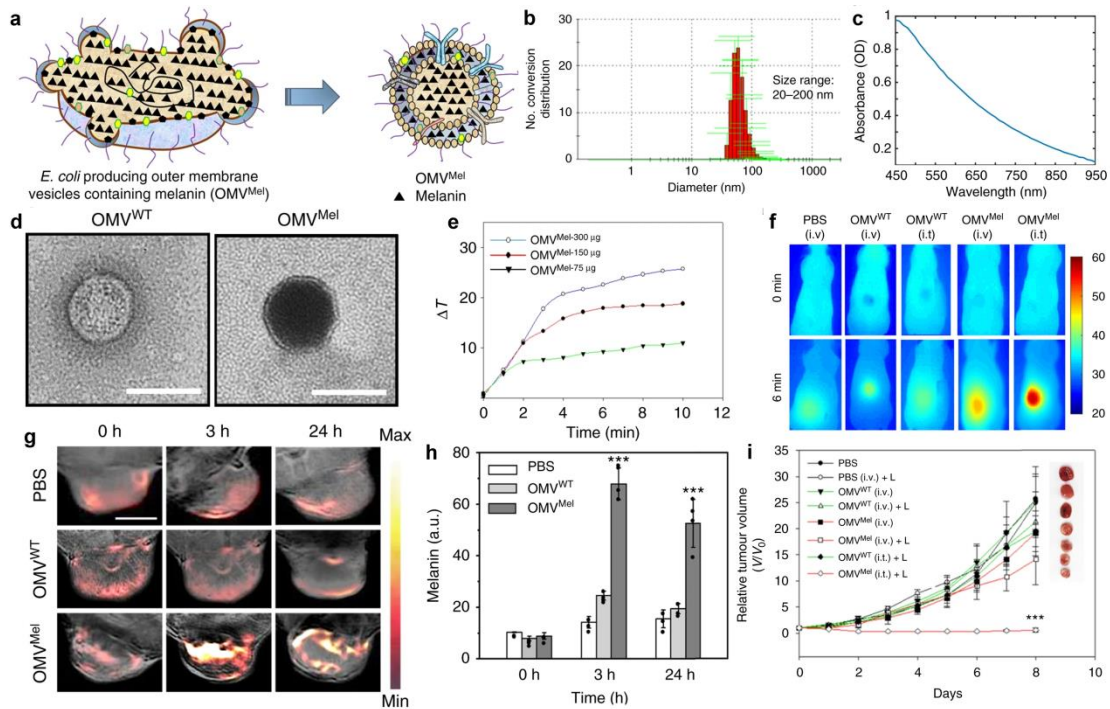


Figure 6 a) Schematic illustration for the generation of OMV^{Mel}. b) Dynamic light scattering analysis of OMV^{Mel}. c) Absorbance spectra of OMV^{Mel}. d) TEM images of OMV^{Mel} and OMV^{WT}. Scale bars, 100 nm. e) Temperature changes of the indicated samples during the exposure to 750 nm laser (0.65 W/cm²) over 10 min. OMV^{WT} represents wild-type outer membrane vesicles. f) Infrared thermal images of indicated 4T1 tumor-bearing mice before and after irradiation of 800 nm laser at 1.5 W/cm² for 6min. g) PAI of 4T1 tumor-bearing mice treated with tail vein injection of indicated samples. Scale bars, 4 mm. h) Concentration of melanin in the tumor over time. i) Tumor growth curves (n=4). ****p* < 0.001.⁷⁷

In addition to cancer diagnosis, therapeutic monitoring is very important to the treatment outcome of cancer diseases as well. Dynamic contrast enhanced (DCE) is helpful to evaluate the functional changes of vessels after therapeutic treatment,⁷⁸ and agents with small size can be used to assess the vessel permeability changes of cancer tissues upon antiangiogenic treatments.⁷⁹ Inspired by this, Longo et al. prepared a highly water-soluble melanin free-acid (MFA) nanoparticles with a hydrodynamic size of 6.9 nm through treating synthetic melanin granules with H₂O₂ in ammonia buffer at pH 7 for a short period of time.¹² The obtained MFA was modified with NH₂-PEG3000-NH₂ to further improve dispersibility. MFA-PEG with a size of 10.5 nm was slightly larger than serum albumin,

thus being suitable to monitor the vessel permeability changes by DCE-PAI of tumor vasculature, which provides an alternative approach for noninvasive assessment of the changes in tumor vasculature after therapeutic treatment.

4.2 Melanin-Based Contrast Agents for MRI of Cancer

MRI is currently a powerful prominent tool for biological molecular imaging and clinical diagnosis because of its superior properties such as high spatial resolution, deep tissue penetration, no ionizing radiation, excellent soft tissue contrast.⁸⁰ Contrast agents for MRI are capable of specifically labeling targets and improving the contrast ratio of target to background, thus enhancing the specificity and accuracy of MRI. Because of the excellent biocompatibility and inherent metal ion chelating capacity, melanin-based nanoplateforms have potential to be conveniently transferred into nano-sized contrast agents for MRI when chelating the metal ions such as Gd^{3+} , Mn^{2+} .

For instance, Cai et al. have synthesized ultrasmall spherical melanin nanoparticles (MNP) via the abovementioned method¹⁴ to chelate Gd^{3+} for preparing melanin based MRI contrast agents.⁸¹ The chelation was conveniently achieved by stirring mixture of MNP and Gd^{3+} at 40 °C for 1 h. ICP-MS revealed that one single MNP was able to maximally chelate 112 Gd^{3+} , which was estimated by the ratio between the amounts of metal and nanoparticles in ICP-MS analysis. Then, the MNP-Gd was used to label bone mesenchymal stem cells (BSC) to track the BSC in vivo via 3.0T MRI. MNP-Gd possessed a T1 relaxivity of 1.97 $mM^{-1}s^{-1}$ and was able to label 97.1% BSC. The MRI signals of MNP-Gd labeled BSC could be still tracked in vivo at 1 month after intramuscular injection. Moreover, MNP-Gd exhibited a modest r_2/r_1 value of 5.27 suggesting that Gd-MNP could be further used as a T1/T2 dual-mode contrast agent, which is helpful to decrease interferences in T1/T2 dual-mode MRI.⁸²

Moreover, melanin-based materials were also used to chelate Mn^{2+} to construct complementary MRI contrast agents to Gd-based contrast agents for in vivo cancer 3.0T MRI.⁸³ In this work, one single MNP could chelate 55 Mn ion, and the chelation was stable that only 1% Mn^{2+} was released over 48 h. The T1 relaxivity of MNP-Mn was 20.57

$\text{mM}^{-1}\text{s}^{-1}$, which was 3.4-fold higher than that of commercial Gadodiamide. After intravenous injection, the MNP-Mn accumulated in the tumor region at 0.5 h post-injection *via* EPR effects and was gradually eliminated at 24 h post-injection due to the metabolism. The biodistribution evidences revealed that liver and kidney played a leading role in excretion of MNP-Mn and most of the MNP-Mn could be cleared in 5 days.

4.3 Melanin-Based Nanoprobes for Multimodality Imaging of Cancer

In comparison with single-modality imaging approaches, multimodality imaging is capable of integrating the innate advantages of different imaging modalities together, thus providing complementary information for precise diagnosis. For instance, MRI and computed tomography (CT) can respectively provide soft tissues contrast and anatomical imaging with high spatial resolution, but limited biological functional information. PET is able to sensitively provide biochemical information of whole body including the level of metabolism and distribution of specific biomarkers.⁸⁴ Hence, combination of PET and MRI/CT can noninvasively provide both biological functional information and anatomical/tissue imaging, thereby playing an important role in clinical diagnosis of cancers, central nervous system diseases, and cardiovascular diseases.⁸⁵⁻⁸⁸ By parity of reasoning, rational design of multimodality imaging approaches would facilitate the advance of clinical cancer diagnosis. To date, lots of rationally designed multimodality imaging nanoprobes have been prepared for cancer imaging, but the synthesis of these multimodality imaging nanoprobes is generally complicated and time-consuming. Because of the promising innate capabilities of generating photoacoustic signal and chelating metal ions, melanin-based nanoplateforms can be conveniently transferred into multimodality imaging nanoprobes for cancers.

In the aforementioned intriguing work,¹⁴ Fan and colleagues have synthesized ultrasmall water-soluble MNP by the way of dissolving pristine melanin granule into alkaline solution⁸⁹ and followed by neutralizing with assistance of sonication to reduce inter-chain aggregation. Then, these nanoparticles were employed in chelation of metal ions ($^{64}\text{Cu}^{2+}$, Fe^{3+}) to be transferred into a novel multifunctional and easily prepared nanoprobe

with integrated different imaging modalities (Figure 7a). To preserve the water-solubility from the influence of metal ion chelation, cross-linking groups with long PEG chains $\text{NH}_2\text{-PEG}_{5000}\text{-NH}_2$ were primarily introduced onto the surface of MNP via dopamine chemistry to further enhance their water-solubility. Furthermore, this cross-linking group could be also used for further biomodification to enhance the tumor targeting capacity of MNP, e.g. linking RGD peptides to confer tumor $\alpha_v\beta_3$ integrin-targeting ability on MNP. The obtained MNP-PEG showed a small hydrodynamic size of 7.0 nm (Figure 7b and 7c) and contained 19 PEG chains per MNP. The RGD-linking enabled one MNP to attach eight RGD peptides on average, which increased the hydrodynamic size to 9.6 nm. The modified MNPs possessed capacity of maximally chelating 100 Cu^{2+} or 90 Fe^{3+} per MNP (Figure 7d) on the basis of ICP-MS analysis. In neutral condition, the chelation was so stable that only 3% Cu^{2+} and 7% Fe^{3+} released from MNPs in 2 h due to the weak electrostatic interaction, and then no further release was observed. Hence, MNPs exhibited potential to be a PAI/PET/MRI integrated nanoprobe for in vivo cancer imaging. In the case of PAI, quantification of photoacoustic signal was performed by the measurement of photoacoustic signal intensity in the region of interest in the PAI images. The analysis results showed that intravenously injected MNP-PEG-RGD enabled a significant increase of photoacoustic signal in tumor site of U87MG tumor-bearing mice at 4 h post-injection compared with that of 0 h (Figure 7e and 7f). The similar signal increase was also observed in MRI of U87MG tumor model. Fe^{3+} -loaded MNP-PEG-RGD exhibited an r_1 value of $1.2 \text{ mM}^{-1}\text{s}^{-1}$, and the relative MR signal intensity of tumor site increased 30% at 4 h post-injection compared with that at 0 h (Figure 7g). In the case of PET imaging, the $^{64}\text{Cu}^{2+}$ -loaded MNP-PEG-RGD enabled a clear tumor contrast at 2 h post-injection, and the tumor uptake value was 4.75% ID/g. Moreover, the uptake could gradually increase to 5.93% ID/g in 24 h post-injection (Figure 7h). Integration of the three imaging modalities could retain the similar imaging properties described above. The accumulation of MNP-PEG-RGD in tumor sites should be attributed to the synergistic effects of $\alpha_v\beta_3$ integrin targeting ability and EPR effects. Notably, PET imaging of MNP-PEG-RGD further proved that MNPs were mainly eliminated by liver and partly by kidney (Figure 7i). This intriguing work has given an

evidence that melanin-based nanoplatforms could be conveniently transferred into a multimodality imaging nanoprobe.

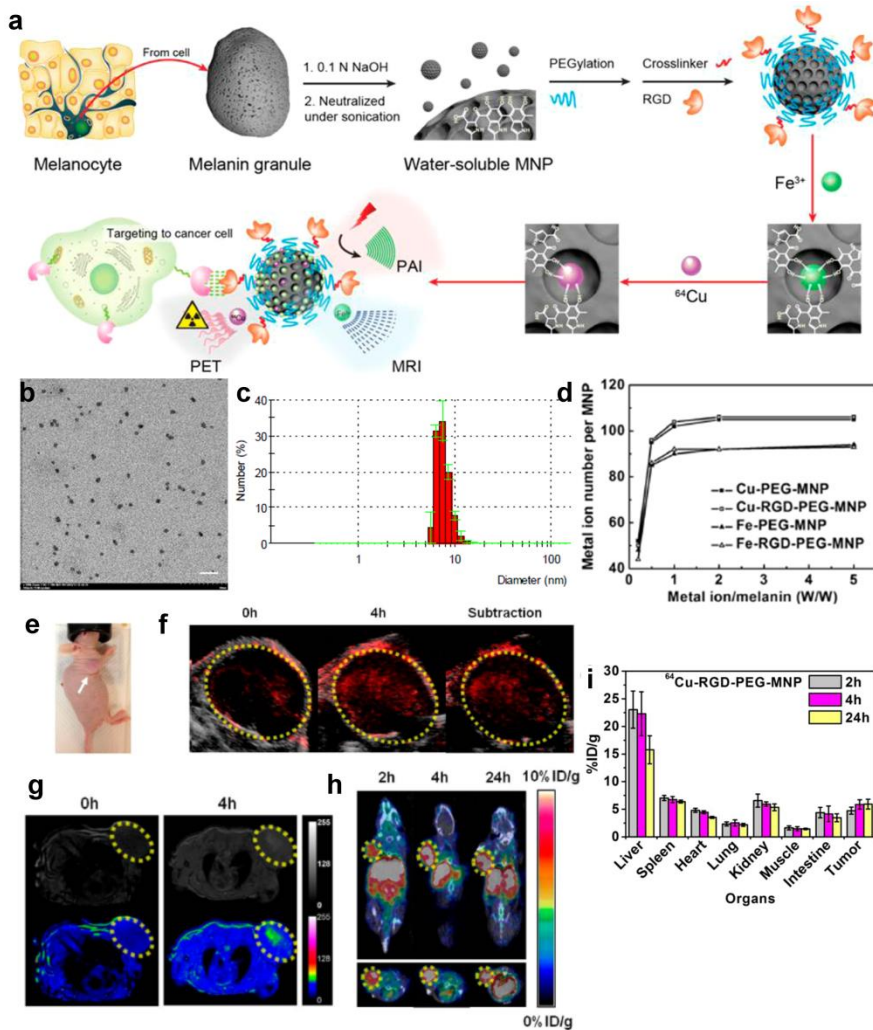


Figure 7 a) Schematic illustration for the preparation and applications of melanin-based multimodality imaging nanoprobe. b) TEM image of MNP-PEG. Scale bar, 20 nm. c) Hydrodynamic size distribution of MNP-PEG. d) Plot of the amounts of chelated metal ions versus feed ratio. e) Photograph of U87MG tumor bearing mice. f) PAI of U87MG tumor bearing mice before and 4 h after tail vein injection of melanin-based PAI/PET/MRI multimodal imaging nanoprobe and their subtraction imaging. g) MRI images of U87MG tumor bearing mice before and 4 h after tail vein injection of melanin-based PAI/PET/MRI multimodal imaging nanoprobe. h) PET imaging of U87MG tumor bearing mice at 2, 4, and 24 h after tail vein injection of melanin-based PAI/PET/MRI multimodal imaging nanoprobe. i) Biodistribution of ^{64}Cu -labeled MNP-PEG-RGD in tumor-bearing mice at the indicated time points post-injection, $n=3$.¹⁴

To further improve the MRI sensitivity of MNPs, this group has prepared a biocaged melanin-based nanoplatform to load more Fe^{3+} for cancer imaging by embedding the ultrasmall MNP into apoferritin.⁹⁰ Apoferritin was a storage protein capable of capturing iron and recognizing transferrin receptor 1 (TfR1), which was overexpressed in many types of cancer cells. In addition, apoferritin possessed the properties of pH-responsive dissociation-reassemble,⁹¹⁻⁹³ and its inside cavity diameter was about 8 nm which was larger than that of MNPs (~4.0 nm). Thus, apoferritin could conveniently encapsulate MNPs within the cavity to construct an apoferritin-MNP complex (AMF) for loading more Fe^{3+} . Fe^{3+} -loading AMF nanoparticles were prepared by mixing the apoferritin, MNPs, and Fe^{3+} together in an acidic solution (pH=2) and then adjusting the pH to 8-10. The AMF nanoparticles showed a much higher Fe^{3+} -loading efficiency (molar ratio of 1:800, AMF: Fe^{3+}) than that of MNPs (molar ratio of 1:90, melanin: Fe^{3+}), which was preferred in MRI due to the positive association between the amount of ferric ion and MR signal. In this case, r_1 value of AMF was $2.54 \text{ mM}^{-1} \text{ s}^{-1}$, which was 2 fold compared to that of MNPs, thus enhancing the MRI sensitivity. AMF nanoparticles exhibited a core-shell structure with a hydrodynamic diameter of 16.4 nm and a zeta potential of -18.4 mV, and could be stable in neutral condition (pH 7.4). Furthermore, combination of the TfR1-targeting ability of apoferritin with the intrinsic photoacoustic properties and $^{64}\text{Cu}^{2+}$ -chelation ability of MNPs enabled AMF nanoparticles to become a TfR1-specific nanoprobe for in vivo TfR1-overexpressing tumor multimodality imaging. In this work, $^{64}\text{Cu}^{2+}$ could be loaded into AMF nanoparticles through multichannels of apoferritin (<1 nm) at slightly acidic condition (pH 6.0). About 80% $^{64}\text{Cu}^{2+}$ has been loaded into AMF after 30 min incubation, and less than 10% loaded $^{64}\text{Cu}^{2+}$ was released from AMF in 24 h. Subsequently, the obtained AMF nanoparticles were intravenously injected into HT29 (TfR1 overexpressed) and HepG2 (low TfR1 expression) tumor models for comparative study. The in vivo experimental results suggested that the significant differences in signal intensity of PET/MRI/PAI between HT29 and HepG2 models could be observed in 4 h after injection. Similar to the MNPs, intravenously injected AMF nanoparticles were then mostly cleared by liver. In addition to chelation of ferric iron for MRI, Hong et al. developed a similar

melanin-based nanoprobe for multimodality imaging (PAI/PET/MRI) by chelating Gd^{3+} for MRI.⁹⁴ The chelation of Gd^{3+} exhibited an excellent stability in buffers with different pH values over 48 h, even in the buffers containing excess metal chelator 1,4,7,10-tetraazacyclodecane-1,4,7,10-tetraacetic acid (DOTA).

In addition to the PAI/PET/MRI three modality imaging, melanin-based nanoplatforms could also be used as nanoprobes for SPECT/MRI/CT imaging when simultaneously complexed positive ions of I^+ , Bi^{3+} , and Fe^{3+} .⁹⁵ In this work, multiple ion doped melanin nanoparticles (iMNP) were prepared by mixing the 100 nm synthetic melanin nanoparticles with Fe^{3+} , Bi^{3+} , and radioactive I^+ (^{125}I or ^{131}I) in sequence (Figure 8a). In this case, 1 mg MNP could combine 2.5-2.7 μmol ions (Figure 8b). Then, the obtained iMNP were further modified with epidermal growth factor receptor (EGFR) antibody and PEG on the surface to acquire EGFR-targeting ability and enhanced solution stability (Figure 8c). The synergistic effects of EGFR-targeting and EPR effects enabled iMNP to target the EGFR-positive tumor site in vivo for SPECT/CT/MRI multimodality imaging (Figure 8d-f). Moreover, the iMNP had the potential be used as a theranostic nanoplatform when ^{131}I was used for complexing.

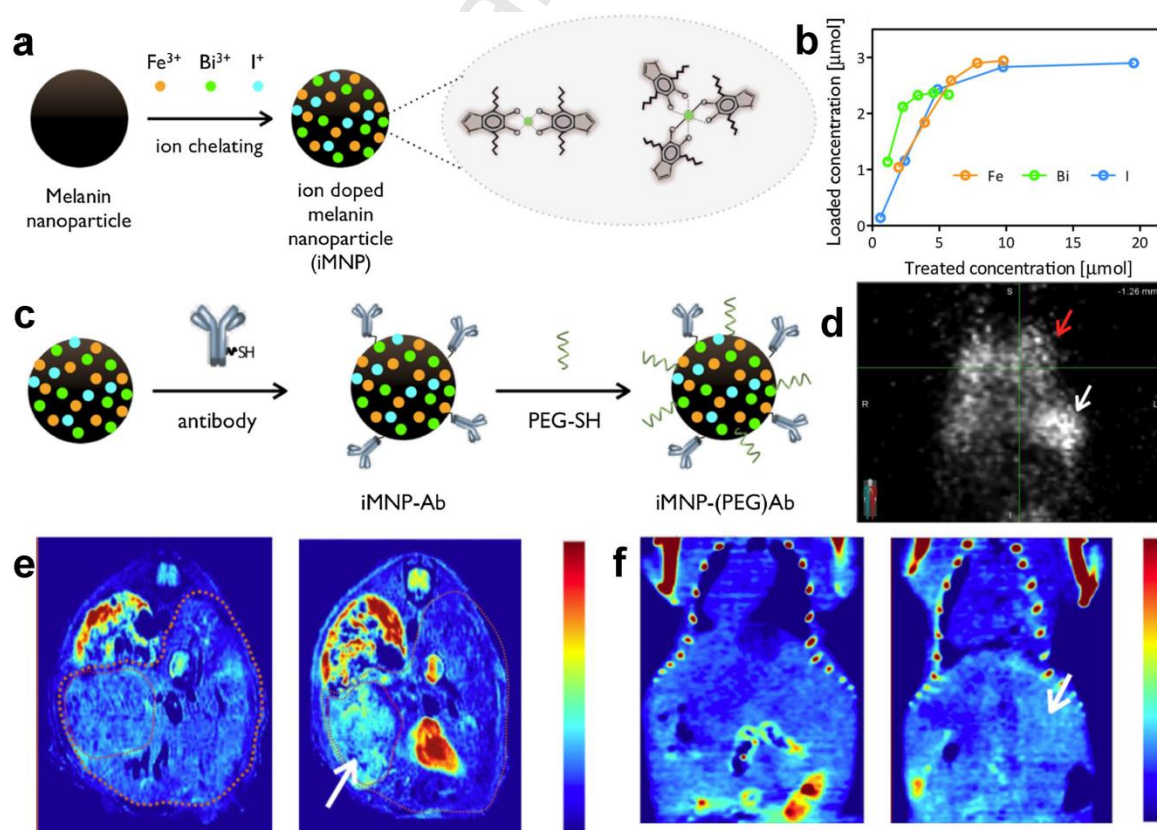


Figure 8 a) Schematic illustration for the preparation of iMNP. b) Plot of ion loading capacity of MNPs. c) Schematic illustration of the surface modification of iMNP with antibody and PEG. d) SPECT imaging of EGFR-positive tumor-bearing mice after 24 h post-injection, coronal projection view. e) MRI of tumor-bearing mice before injection (left) and after 24 h post-injection (right), axial view. f) CT imaging of tumor-bearing mice before injection (left) and after 24 h post-injection (right), coronal view. White arrows indicated tumor in liver while red arrow indicated normal lung.⁹⁵

Besides the inherent photoacoustic properties, melanin-based nanomaterials could also generate fluorescence when excited by the light with the wavelength around 600 nm. Combination of the two optical properties could achieve PAI/fluorescence imaging.⁹⁶ However, the relatively short fluorescence emission wavelength (around 650 nm) may be an issue to be considered about before its clinical applications due to the light absorption and scattering in tissues.

5. Melanin-Based Nanoplatfoms for Cancer Theranostics

Integrating the functionalities of diagnosis and therapy together into a single agent was determined as theranostics, which is becoming an attractive approach for cancer diagnosis and treatments. As mentioned above, melanin-based nanoplatfoms are biocompatible and have innate advantages in integrating imaging and therapeutic functionalities, thus having potential to enhance diagnostic accuracy and therapy efficacy of cancers. To date, melanin-based nanoplatfoms have been popularly used for constructing theranostic agents for cancer diagnosis and therapy.

The inherent photothermal conversion ability enabled melanin-based materials to be an inborn theranostic nanoplatfom for PAI and PTT of cancers. Moreover, red blood cell (RBC) membrane was a promising candidate for modifying the surface of nanoparticles to enhance their blood retention and accumulation in cancer tissues,^{97, 98} thus being favorable to improve the efficacy of PAI and PTT of melanin-based nanomaterials in tumor site. Hence, Jiang and co-workers took advantages of these properties to construct a RBC membrane coated melanin-based nanoparticles (Melanin@RBC) for in vivo PAI guided

cancer PTT (Figure 9a).⁹⁹ In this work, spherical natural melanin nanoparticles with an average diameter of 128 nm were extracted and purified from freshly dissected ink sac of cuttlefish, and then were further coated with RBC membrane through an extrusion approach based on 200 nm polycarbonate porous membrane. The modification of RBC membrane was verified by the absorbance peak at 420 nm (Figure 9b) and the presence of CD47 protein in Melanin@RBC. This modification made melanin nanoparticles less negatively charged (Figure 9c) and increased their size by 16 nm, which indicated two layers of RBC membrane (~7.8 nm per membrane) were modified onto the surface of melanin nanoparticles. Moreover, the RBC membrane-coating induced no significant effects on the photothermal property of melanin nanoparticles (Figure 9d) and exhibited a photothermal conversion efficiency of 40%, which was higher than that of synthetic PDA nanoparticles (29%). Importantly, the RBC membrane modification increased 10-fold blood retention of melanin nanoparticles at 24 h after intravenous injection (Figure 9e). Using A549 tumor-bearing mice as a study model, intravenously injected Melanin@RBC nanoparticles could achieve the PAI of tumor site due to EPR effects. The photoacoustic signal of tumor site was gradually increased within 4 h and peaked at 4 h post-injection (Figure 9f and 9g). In 4 h post-injection, Melanin@RBC group exhibited an enhanced photoacoustic signal than melanin group (Figure 9f), which was attributed to the tumor accumulation enhancement of nanoparticles induced by RBC membrane modification. More accumulation of melanin in tumor site could generate more heat for tumor ablation upon laser irradiation (Figure 9h), thus improving the therapeutic effects on cancers (Figure 9i and 9j). In this case, the Melanin@RBC nanoparticles were of a good antitumor PTT efficacy that tumor ablation could be observed even at a low laser power density of 1 W/cm² for 10 min (Figure 9i and 9j). In consistent with abovementioned work, the injected melanin-based nanoparticles were mostly eliminated via liver and spleen.

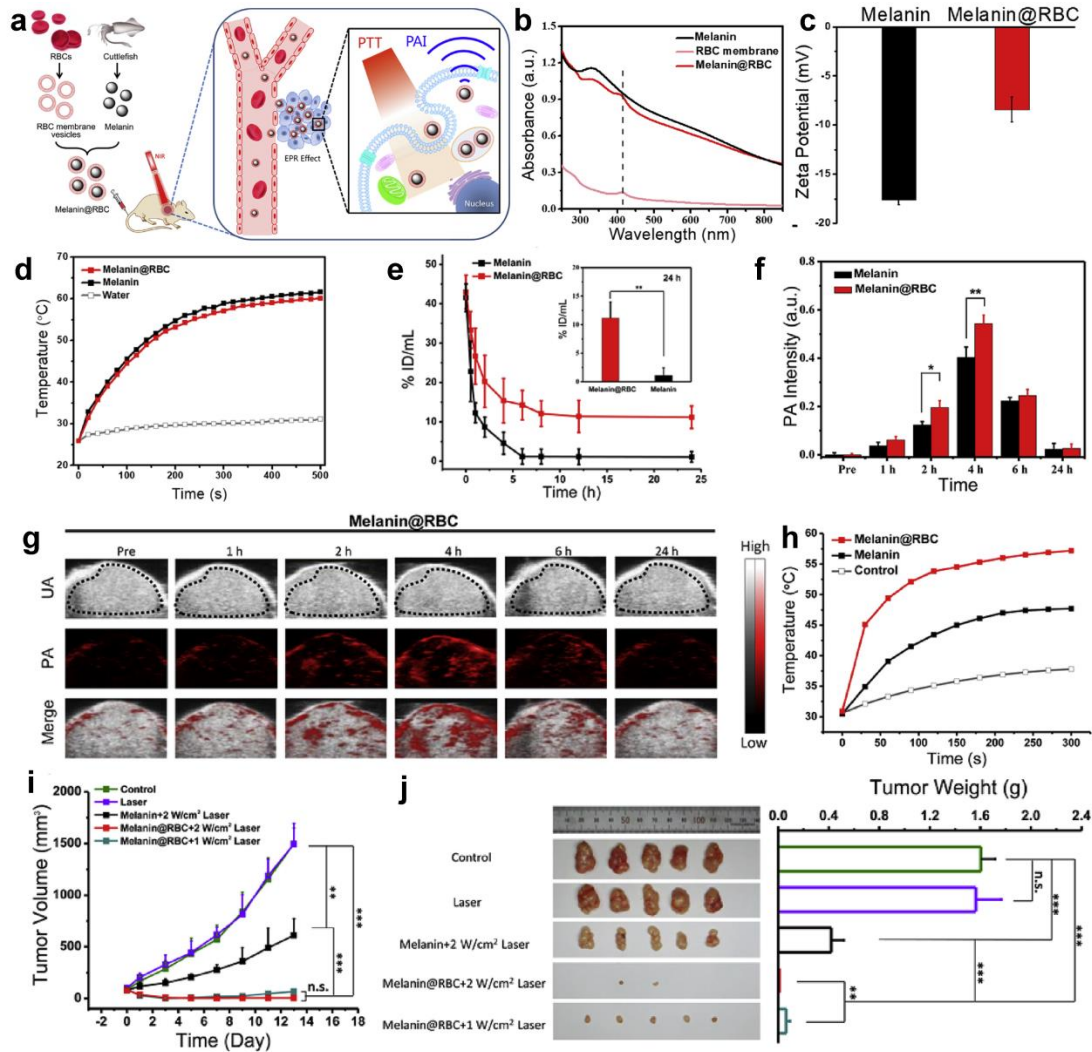


Figure 9 a) Schematic illustration of Melanin@RBC for PAI guided cancer PTT. b) Absorbance spectra of indicated samples. c) Zeta potential of Melanin@RBC and melanin nanoparticles. d) Temperature changes of Melanin@RBC nanoparticles and melanin nanoparticles at the same concentration upon 808 nm laser irradiation. e) Blood retention of the intravenously injected Melanin@RBC and melanin nanoparticles over 24 h, $n=4$. The inset exhibited the blood retention of the nanoparticles at 24 h post intravenous injection. f) Photoacoustic signal intensity of the tumor region in the A549 tumor-bearing mice that intravenously injected with Melanin@RBC and melanin nanoparticles, $n=3$. g) PAI, ultrasound (UA) imaging, and their merged images of tumor region at different time after intravenous injection of Melanin@RBC. h) Tumor temperature evaluation curves vs time. i) Tumor volume changes of A549 tumor-bearing mice after indicated treatments. j) Comparison of the tumors dissected from the tumor-bearing mice on the 13th day after indicated treatments, $n=5$. * $p < 0.05$, ** $p < 0.01$, *** $p < 0.001$.⁹⁹

As mentioned in above sections, melanin-based nanoplatfoms are capable of chelating metal ions for MRI or PET imaging and binding drugs for CHT. Combination of the imaging modalities with PTT and/or CHT could provide possibilities for in vivo cancer multimodality theranostics, e.g. MRI guided cancer PTT.¹⁰⁰ In an intriguing work, Strizker and co-workers employed genetic engineering technology to enable cancer cells to overexpress melanin to achieve in vivo in situ cancer theranostics.¹⁰¹ On the basis of the previous study that vaccinia virus strain was effective in treating cancers and has completed phase I clinical trials,¹⁰² the key genes in melanogenesis were inserted into a vaccinia virus strain so as to introduce melanogenesis into cancer cells, and then the overproduction of melanin enabled in situ PAI and PTT of tumor tissues. Moreover, the endogenous melanin had possibilities to directly achieve T1-weighted MRI due to the possible chelation of paramagnetic transition metal ions.¹⁰³ After analyzing several gene engineered vaccinia virus strain, GLV-1h324 exhibited a relatively more efficient expression of melanin in cells. More melanin production could enhance the absorption of NIR light, which would then be transferred into thermal energy for more temperature rising capable of enhancing the PTT efficacy of cancers. This was established by the temperature rising of melanin-expressed cells induced by the irradiation of NIR laser. Results indicated that GLV-1h324 infected cells could increase by 41 °C after 2 min exposure to the NIR laser light, which was much higher than that of cells infected by other types of GLV (25 °C for GLV-1h327). According to the principle of PAI, the photothermal conversion enabled the production of photoacoustic signal for PAI of melanin overexpressed cancer cells. Furthermore, due to the possible chelation of paramagnetic transition metal ions, the melanin overexpressed cancer cells could be also imaged by MRI and herein the GLV-1h324 strain exhibited a relatively good T1 shortening. This work provided an alternative approach to enable self-synthesis of melanin in vivo for cancer theranostics.

In addition to the MRI guided cancer therapy, multimodality imaging guided drug delivery could be conveniently achieved by melanin-based nanoplatfoms. On the basis of their previous work,¹⁴ Zhang et al. utilized the ultrasml PEG-modified MNPs with a size of 7.5 nm as a nanoplatfom to chelate $^{64}\text{Cu}^{2+}$ and bind an FDA-approved multikinase

inhibitor SRF for in vivo PAI/PET guided drug delivery (Figure 10a).¹⁶ In this work, the SRF-binding induced the self-aggregation of PEG-modified MNPs to form relatively large nanoparticles with a size of 60 nm (Figure 10b and 10c) since the hydrophobic drug-binding decreased the hydrophilicity of MNPs. On the basis of analyzing the characteristic absorption peak of SRF at 275 nm, results indicated that 1.0 mg MNPs was able to bind 0.25 mg SRF. The release behaviors of SRF bound to MNPs were very similar at pH 7.2 and 5.0 (Figure 10d). After rapidly releasing the 18% of SRF that physically absorbed in the initial 2 h, the rest of SRF were gradually released in a slow speed. In this case, about 40% SRF was released in 24 h and nearly 80% SRF was released in 72 h. Moreover, the aggregation decreased the surface-to-volume of MNPs and also reduced the chelation sites for metal ions, thereby decreasing the yield of $^{64}\text{Cu}^{2+}$ labeled MNPs to 64% compared to the 80% in their previous work. Notably, the chelation was still stable, and only 3% $^{64}\text{Cu}^{2+}$ was released from MNPs after incubation in PBS for 24 h. The chelation of $^{64}\text{Cu}^{2+}$ enabled the biodistribution analysis of SRF-MNPs that were injected into HepG2-tumor-bearing mice via tail-vein injection. PET/CT imaging showed that accumulation of SRF-MNPs in the tumor tissues peaked at 4 h post-injection and then decreased by 13% at 24 h (Figure 10f). Although there was about 20% loss of SRF before the time point of highest accumulation of SRF-MNPs in tumor site (Figure 10d), the remaining SRF could still gradually release from SRF-MNPs for cancer therapy. In addition, the biodistribution analysis based on the PET/CT imaging also revealed that SRF-MNPs were mostly cleared via liver and spleen (Figure 10g), which agreed with the previous studies. Then, PAI upon the irradiation of 680 nm laser was used to evaluate the SRF-MNPs in the blood vessel around the superficial area of tumor tissue. According to the photoacoustic signal intensity of tumor site (Figure 10e and 10h), the photoacoustic signal of tumor increased in the first 4 h and then decreased at 24 h post-injection. The authors deemed that the decrease of photoacoustic signal at 24 h post-injection should be attributed to the penetration of SRF-MNPs into inner region of tumor, which would be helpful to the therapeutic effect enhancement. Subsequently, a comparative study with duration of 20 days was performed to evaluate the therapeutic effect of SRF-MNP treatment on cancer

disease (Figure 10i). Results of the study indicated that the SRF-MNP treatment by tail-vein injection exhibited a better effect on suppression of HepG2-tumor growth than oral SRF treatment (Figure 10i and 10j). In this case, MNP was a promising nanoplatform for SRF delivery to lower the side effects of SRF.

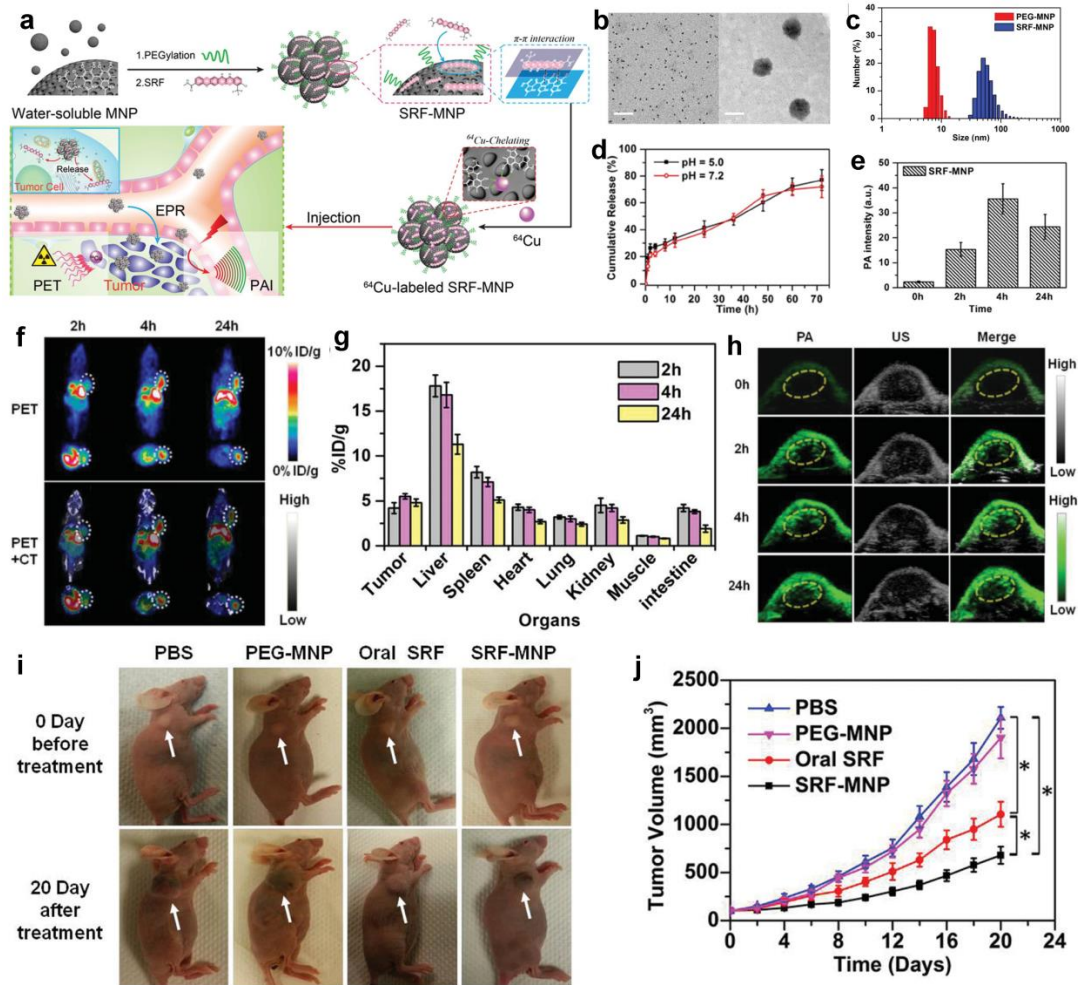


Figure 10 a) Schematic illustration of the preparation and application of SRF-MNPs in cancer theranostics. b) TEM images of PEG-modified MNPs (left) and SRF-MNPs (right). scale bar, 50 nm. c) Hydrodynamic size of PEG-modified MNPs and SRF-MNPs. d) Release of SRF from SRF-MNP at pH=7.2 and 5.0 as a function of time. e) Photoacoustic signal intensity of the tumor region in the HepG2 tumor-bearing mice at indicated time points after intravenous injection of SRF-MNPs (n=3). f) PET/CT imaging of HepG2 tumor-bearing mice at 2, 4, and 24 h after tail vein injection of ^{64}Cu -radiolabeled SRF-MNPs. g) Biodistribution of ^{64}Cu -radiolabeled SRF-MNPs in mice at 2, 4, and 24 h after tail vein injection (n = 3). h) PAI, UA, and their merged images of HepG2 tumor at different time points after intravenous injection of SRF-MNPs in living mice. i) Photographs of HepG2 tumor-bearing mice before

and 20 days after the treatments of intravenously injected PBS, PEG-modified MNPs, and SRF-MNPs as well as oral treatment with SRF. j) Tumor volume changes of HepG2 tumor-bearing mice versus time after the indicated treatments ($n = 6$). $*p < 0.05$.¹⁶

Combination of PTT with gene therapy is a promising multimodality therapy in cancer treatments, and has attracted much attention.¹⁰⁴ Imaging guided multimodality therapy could be helpful to enhance the accuracy and efficacy of cancer treatments. The innate talents of melanin-based nanoplateforms enabled them to be flexible in constructing theranostic nanoagents for imaging guided multimodality therapy. Recently, Fan and co-workers designed a microRNA-loaded MNPs for PAI guided thermo-gene therapy.¹⁰⁵ The MNPs prepared according to the aforementioned typical method¹⁴ were modified with poly-L-lysine (PLL) on the surface, which enabled the surface of MNPs to be covered with positive charges for subsequent microRNA binding. The surface modification increased zeta potential of MNPs from -36.5 mV to +53.1 mV. Then, a kind of microRNA named miR-145-5p, which was capable of inhibiting cancer cell migration and inducing cancer cell apoptosis,^{106, 107} was bound to the surface of the positively charged MNPs through electrostatic binding. The binding decreased the positive charges, and the obtained nanoparticles (MNP-PLL-miRNA) had a zeta potential of +5.56 mV. The innate photothermal conversion ability of MNPs not only enabled PTT of cancers, but also could accelerate miRNA release here. In this work, NIR irradiation could result in 55.2% miRNA release, much more than the release value of control group that without NIR irradiation (3.28%). To optimize the time point of PTT, MNP-PLL-miRNA nanoparticles were intratumorally injected into the Hep2-bearing tumor mice. In vivo photoacoustic imaging suggested that the photoacoustic signal intensity of tumor region peaked at 4 h post-injection. Therefore, PTT of tumor region was administered at the time point of 4 h post-injection. The photothermal conversion resulted from 5 min irradiation of 1.5 W/cm² NIR laser could increase the tumor temperature from 35.0 to 57.6 °C, hence capable to kill cancer cells and accelerate miRNA release. Moreover, results of comparative study established that tumor was efficiently ablated via PTT and the presence of miR-145-5p

played an important role in suppression of tumor recurrence.

The versatility of melanin-based nanoplatforms provides themselves the possibilities to integrate functions of multimodality imaging and multimodality therapy into one single nanoagent. For example, Wang et al. have synthesized spherical PEGylated PDA nanoparticles via typical method for loading of Fe^{3+} and IR820 to fabricate a biocompatible nanoagent (PPIF) for multimodality imaging and therapy.¹⁰⁸ Herein, 1 mg PPIF nanoparticles chelated 14.8 μg iron ions capable to be used as MRI agents. IR820 was a cyanine dye that had absorption in NIR region, and has been widely used in cancer imaging guided phototherapies because of its excellent optical properties and high photo-conversion efficiency upon NIR irradiation.¹⁰⁹ In this work, IR820 was bound to the PDA nanoparticles through π - π /electrostatic interactions to provide enhancements in signal intensity of PAI and efficacy of cancer phototherapy for PDA nanoparticles. The loading ratio of IR820 was more than 60% when the feed ratio between IR820 and PDA nanoparticles (w/w) was 0.06/1. In this case, upon the irradiation of 706 nm laser pulse, the PPIF nanoparticles exhibited a stronger photoacoustic signal intensity than the PDA nanoparticles without IR820 at the same concentration. This was explained that the absorbance of IR820 at 706 nm generated photoacoustic signals, thus enhancing the overall photoacoustic signal intensity of PDA nanoparticles. In addition, loading of IR820 achieved an enhancement of ROS generation as well as photothermal conversion for PDA nanoparticles. The ROS generated by PPIF could be used for photodynamic therapy (PDT) of cancers. Combination of the PDT and PTT could improve the ablation of cancer cells, which was established by the in vitro experimental results. Aside from the imaging and therapy modalities presented above, melanin-based materials could also play as a radioactive nanoplatform for cancer theranostics through loading with some theranostic radioactive isotopes. Inspired by clinically used brachytherapy seed of AgI, Sheng et al. constructed a melanin-based radioactive theranostic nanoparticle by loading with a theranostic radioactive isotope ^{131}I for cancer SPECT imaging and radiotherapy.¹¹⁰ In this work, MNPs were prepared via the aforementioned typical method,¹⁴ and then chelated Ag^+ for labeling of ^{131}I to fabricate theranostic nanoagent (MNP-Ag- ^{131}I). The MNP-Ag- ^{131}I had a small size of 12 nm and

could be stable in saline solution and serum. To investigate the treatment efficacy in vivo, MNP-Ag-¹³¹I and ¹³¹I were intratumorally injected into PC3 tumor-bearing mice for comparative study. In vivo imaging suggested that binding to the nanoparticles could prolong the retention time of ¹³¹I in tumor tissue, thus enhancing the tumor growth suppression ability.

6. Summary and Prospective

In summary, the inherent fascinating properties enable melanin-based materials (including natural melanin and PDA) to be promising building blocks for rational and effective design of nanoagents for cancer diagnosis, therapy, and theranostics. The innate photothermal conversion ability makes melanin-based nanoplatfoms be an inborn theranostic nanoagent for PAI-guided PTT of cancer. The excellent drug-binding ability of melanin-based nanoplatfoms enables them to become DDS for CHT, thus being able to achieve PTT-CHT synergistic therapy of cancers. The robust metal chelating capacity is capable of transferring melanin-based nanoplatfoms into imaging nanoprobos for SPECT, MRI, and PET. High chemical reactivity of the functional groups on the surface of melanin-based materials can realize the conjugation of cancer-targeting biomolecules, thereby enhancing the cancer specificity of melanin-based nanoplatfoms. Moreover, the remarkable adhesive property enables melanin-based materials to conveniently confer their innate talents on the other nanomaterials, thus constructing versatile nanoagents for cancer diagnosis and treatments. This review offers an overview of the applications of melanin-based nanoplatfoms in fundamental researches of cancer diagnosis and treatments. Even though melanin-based nanoplatfoms exhibited impressive potential in medical application, there are remaining challenges need to be overcome for clinical translation in the future. Although it was widely reported that intravenously injected melanin-based nanoparticles were mostly eliminated through hepatobiliary system without significant side effects on organs, systematical investigations on the immunogenicity, degradation mechanism, and long-term toxicity of melanin-based nanoparticles may be still needed before their clinical use. Furthermore, when melanin-based nanomaterials were used for

PAI and/or PTT, the wavelengths of irradiation were mostly in the NIR-I region. Hence, the tissue penetration depth of optical irradiation may make melanin-based nanoparticles be more appropriate to PAI and/or PTT of superficial tumor in clinical use. Thus, integration of multimodality imaging and/or synergistic therapy into one single melanin-based nanoplatform would be more effective in cancer diagnosis and therapy. Despite the remaining hurdles on the road of clinical translation, melanin-based nanoplatforms are expected to play an important role in overcoming the challenges in cancer diagnosis and treatments in the future.

References

1. Allemani C, Matsuda T, Di Carlo V, Harewood R, Matz M, Niksic M, et al. Global surveillance of trends in cancer survival 2000-14 (CONCORD-3): analysis of individual records for 37 513 025 patients diagnosed with one of 18 cancers from 322 population-based registries in 71 countries. *Lancet* 2018; **391**: 1023-75.
2. Chen H, Gu Z, An H, Chen C, Chen J, Cui R, et al. Precise nanomedicine for intelligent therapy of cancer. *Sci China Chem* 2018; **61**: 1503-52.
3. Simon JD. Spectroscopic and dynamic studies of the epidermal chromophores trans-urocanic acid and eumelanin. *Acc Chem Res* 2000; **33**: 307-13.
4. Meredith P, Sarna T. The physical and chemical properties of eumelanin. *Pigm Cell Res* 2006; **19**: 572-94.
5. Hong L, Simon JD. Current understanding of the binding sites, capacity, affinity, and biological significance of metals in melanin. *J Phys Chem B* 2007; **111**: 7938-47.
6. Ren G, Miao Z, Liu H, Jiang L, Limpa-Amara N, Mahmood A, et al. Melanin-targeted preclinical PET imaging of melanoma metastasis. *J Nucl Med* 2009; **50**:1692-99.
7. Bu L, Li R, Liu H, Feng W, Xiong X, Zhao H, et al. Intrastratial transplantation of retinal pigment epithelial cells for the treatment of parkinson disease: In vivo longitudinal molecular imaging with F-18-P3BZA PET/CT. *Radiology* 2014; **272**: 174-83.
8. Cheng Z, Mahmood A, Li HZ, Davison A, Jones AG. 99(m)TcOAAADT-(CH₂)₂-NEt₂: A potential small-molecule single-photon emission computed tomography probe for imaging metastatic melanoma. *Cancer Res* 2005; **65**: 4979-86.
9. Fabbri M, Reimao S, Carvalho M, Nunes RG, Abreu D, Guedes LC, et al. Substantia nigra neuromelanin as an imaging biomarker of disease progression in parkinson's disease. *J Parkinson Dis* 2017; **7**: 491-501.
10. Ma X, Wang S, Wang S, Liu D, Zhao X, Chen H, et al. Biodistribution, radiation dosimetry, and clinical application of a melanin-targeted PET probe, F-18-P3BZA, in patients. *J Nucl Med* 2019; **60**: 16-22.
11. Perez-Gutierrez FG, Camacho-Lopez S, Evans R, Guillen G, Goldschmidt BS, Viator JA, et al. Plasma Membrane Integrity and Survival of Melanoma Cells After Nanosecond Laser Pulses. *Ann*

- Biomed Eng* 2010; **38**: 3521-31.
12. Longo DL, Stefania R, Callari C, De Rose F, Rolle R, Conti L, et al. Water soluble melanin derivatives for dynamic contrast enhanced photoacoustic imaging of tumor vasculature and response to antiangiogenic therapy. *Adv Healthcare Mater* 2017; **6**: 1600550.
 13. Qin CX, Cheng K, Chen K, Hu X, Liu Y, Lan XL, et al. Tyrosinase as a multifunctional reporter gene for Photoacoustic/MRI/PET triple modality molecular imaging. *Sci Rep-UK* 2013; **3**: 1490-97.
 14. Fan Q, Cheng K, Hu X, Ma X, Zhang R, Yang M, et al. Transferring biomarker into molecular probe: Melanin nanoparticle as a naturally active platform for multimodality imaging. *J Am Chem Soc* 2014; **136**: 15185-94.
 15. Ings RMJ. The melanin binding of drugs and its implications. *Drug Metab Rev* 1984; **15**: 1183-1212.
 16. Zhang R, Fan Q, Yang M, Cheng K, Lu X, Zhang L, et al. Engineering melanin nanoparticles as an efficient drug-delivery system for imaging-guided chemotherapy. *Adv Mater* 2015; **27**: 5063-69.
 17. Huang L, Liu M, Huang H, Wen Y, Zhang X, Wei Y. Recent advances and progress on melanin-like materials and their biomedical applications. *Biomacromolecules* 2018; **19**: 1858-68.
 18. d'Ischia M, Napolitano A, Ball V, Chen CT, Buehler MJ. Polydopamine and eumelanin: From structure-property relationships to a unified tailoring strategy. *Acc Chem Res* 2014; **47**: 3541-50.
 19. Arzillo M, Mangiapia G, Pezzella A, Heenan RK, Radulescu A, Paduano L, et al. Eumelanin buildup on the nanoscale: Aggregate growth/assembly and visible absorption development in biomimetic 5,6-Dihydroxyindole polymerization. *Biomacromolecules* 2012; **13**: 2379-90.
 20. Aime S, Fasano M, Terreno E, Groombridge CJ. NMR-studies of melanins - characterization of a soluble melanin free acid from sepia ink. *Pigm Cell Res* 1991; **4**: 216-21.
 21. Liu YL, Ai KL, Liu JH, Deng M, He YY, Lu LH. Dopamine-melanin colloidal nanospheres: An efficient near-infrared photothermal therapeutic agent for in vivo cancer therapy. *Adv Mater* 2013; **25**: 1353-59.
 22. Ju KY, Lee JW, Im GH, Lee S, Pyo J, Park SB, et al. Bio-inspired, melanin-like nanoparticles as a highly efficient contrast agent for T-1-weighted magnetic resonance imaging. *Biomacromolecules* 2013; **14**: 3491-97.
 23. Hu D, Liu C, Song L, Cui H, Gao G, Liu P, et al. Indocyanine green-loaded polydopamine-iron ions coordination nanoparticles for photoacoustic/magnetic resonance dual-modal imaging-guided cancer photothermal therapy. *Nanoscale* 2016; **8**: 17150-58.
 24. Xi J, Da L, Yang C, Chen R, Gao L, Fan L, et al. Mn²⁺-coordinated PDA@DOX/PLGA nanoparticles as a smart theranostic agent for synergistic chemo-photothermal tumor therapy. *Int J Nanomed* 2017; **12**: 3331-45.
 25. Wang S, Lin J, Wang Z, Zhou Z, Bai R, Lu N, et al. Core-satellite polydopamine-gadolinium-metallofullerene nanotheranostics for multimodal imaging guided combination cancer therapy. *Adv Mater* 2017; **29**: 1701013.
 26. Hong S., Na YS., Choi S, Song IT, Kim WY, Lee H. Non-covalent self-assembly and covalent polymerization co-contribute to polydopamine formation. *Adv Funct Mater* 2012; **22**: 4711.
 27. Xu H, Liu X, Wang D. Interfacial basicity-guided formation of polydopamine hollow capsules in pristine O/W emulsions - toward understanding of emulsion template roles. *Chem Mater* 2011; **23**: 5105.
 28. Crippa PR, Martini F, Viappiani C. Direct evidence of electron phonon interaction in melanins. *J Photoch Photobio B* 1991; **11**: 371.
 29. Szpoganicz B, Gidanian S, Kong P, Farmer P. Metal binding by melanins: studies of colloidal

- dihydroxyindole-melanin, and its complexation by Cu(II) and Zn(H) ions. *J Inorg Biochem* 2002; **89**: 45.
30. Lee H, Dellatore SM, Miller WM, Messersmith PB. Mussel-inspired surface chemistry for multifunctional coatings. *Science* 2007; **318**: 426.
 31. Lee H, Scherer NF, Messersmith PB. Single-molecule mechanics of mussel adhesion. *Proc. Natl. Acad. Sci. U. S. A.* 2006; **103**: 12999.
 32. Liu YL, Ai KL, Lu LH. Polydopamine and its derivative materials: synthesis and promising applications in energy, environmental, and biomedical fields. *Chem Rev* 2014; **114**: 5057.
 33. Vogel A, Venugopalan V. Mechanisms of pulsed laser ablation of biological tissues. *Chem Rev* 2003; **103**: 577-644.
 34. Kievit FM, Zhang M. Surface engineering of iron oxide nanoparticles for targeted cancer therapy. *Acc Chem Res* 2011; **44**: 853-62.
 35. Emelianov SY, Li PC, O'Donnell M. Photoacoustics for molecular imaging and therapy. *Phys Today* 2009; **62**: 34-39.
 36. Choi WI, Kim JY, Kang C, Byeon CC, Kim YH, Tee G. Tumor regression in vivo by photothermal therapy based on gold-nanorod-loaded, functional nanocarriers. *ACS Nano* 2011; **5**: 1995-2003.
 37. Liu Y, Ai K, Liu J, Yuan Q, He Y, Lu L. A high-performance ytterbium-based nanoparticulate contrast agent for in vivo X-ray computed tomography imaging. *Angew Chem Int Edit* 2012; **51**: 1437.
 38. Chu M, Hai W, Zhang Z, Wo F, Wu Q, Zhang Z, et al. Melanin nanoparticles derived from a homology of medicine and food for sentinel lymph node mapping and photothermal in vivo cancer therapy. *Biomaterials* 2016; **91**: 182-99.
 39. Kim M, Kim HS, Kim MA, Ryu H, Jeong HJ, Lee CM. Thermohydrogel containing melanin for photothermal cancer therapy. *Macromol Biosci* 2017; **17**: 1-6.
 40. Li Y, Zhang X, Zheng M, Liu S, Xie Z. Dopamine carbon nanodots as effective photothermal agents for cancer therapy. *RSC Adv* 2016; **6**: 54087-91.
 41. Ding W, Chechetka SA, Masuda M, Shimizu T, Aoyagi M, Minamikawa H, et al. Lipid nanotube tailored fabrication of uniquely shaped polydopamine nanofibers as photothermal converters. *Chem Eur J* 2016; **22**: 4345-50.
 42. Kim SH, Sharker SM, Lee H, In I, Lee KD, Park SY. Photothermal conversion upon near-infrared irradiation of fluorescent carbon nanoparticles formed from carbonized polydopamine. *RSC Adv* 2016; **6**: 61482-91.
 43. Wang T, LaMontagne D, Lynch J, Zhuang J, Cao YC. Colloidal superparticles from nanoparticle assembly. *Chem Soc Rev* 2013; **42**: 2804-23.
 44. Wang T, Zhuang J, Lynch J, Chen O, Wang Z, Wang X, et al. Self-assembled colloidal superparticles from nanorods. *Science* 2012; **338**: 358-63.
 45. Tian Y, Shen S, Feng J, Jiang X, Yang W. Mussel-inspired gold hollow superparticles for photothermal therapy. *Adv Healthcare Mater* 2015; **4**: 1009-14.
 46. Li J, Wang W, Zhao L, Rong L, Lan S, Sun H, et al. Hydroquinone-assisted synthesis of branched Au-Ag nanoparticles with polydopamine coating as highly efficient photothermal agents. *ACS Appl Mater Interfaces* 2015; **7**: 11613-23.
 47. Yu J, Lin YH, Yang L, Huang CC, Chen L, Wang WC, et al. Improved anticancer photothermal therapy using the Bystander effect enhanced by antiarrhythmic peptide conjugated dopamine-modified reduced graphene oxide nanocomposite. *Adv Healthcare Mater* 2017; **6**:

- 1600804.
48. Yang LY, Tseng YT, Suo GL, Chen LL, Yu JT, Chiu WJ, et al. Photothermal therapeutic response of cancer cells to aptamer-gold nanoparticle-hybridized graphene oxide under NIR illumination. *ACS Appl Mater Interfaces* 2015; **7**: 5097.
 49. Meng D, Yang S, Guo L, Li G, Ge J, Huang Y, et al. The enhanced photothermal effect of graphene/conjugated polymer composites: photoinduced energy transfer and applications in photocontrolled switches. *Chem Commun* 2014; **50**: 14345.
 50. Cui JW, Yan Y, Such GK, Liang K, Ochs CJ, Postma A, et al. Immobilization and intracellular delivery of an anticancer drug using mussel-inspired polydopamine capsules. *Biomacromolecules* 2012; **13**: 2225-28.
 51. Mrowczynski R, Jurga-Stopa J, Markiewicz R, Coy EL, Jurga S, Wozniak A. Assessment of polydopamine coated magnetic nanoparticles in doxorubicin delivery. *RSC Adv* 2016; **6**: 5936-43.
 52. Ho CC, Ding SJ. The pH-controlled nanoparticles size of polydopamine for anti-cancer drug delivery. *J Mater Sci: Mater Med* 2013; **24**: 2381-90.
 53. Zavareh S, Mahdi M, Erfanian S, Hashemi-Moghaddam H. Synthesis of polydopamine as a new and biocompatible coating of magnetic nanoparticles for delivery of doxorubicin in mouse breast adenocarcinoma. *Cancer Chemother Pharmacol* 2016; **78**: 1073-84.
 54. Zhu Z, Su M. Polydopamine nanoparticles for combined chemo- and photothermal cancer therapy. *Nanomaterials* 2017; **7**: 160.
 55. Gao Y, Wu X, Zhou L, Su Y, Dong CM. A sweet polydopamine nanoplatform for synergistic combination of targeted chemo-photothermal therapy. *Macromol Rapid Commun* 2015; **36**: 916-22.
 56. Wang X, Wang C, Wang X, Wang Y, Zhang Q, Cheng Y. A polydopamine nanoparticle-knotted poly(ethylene glycol) hydrogel for on-demand drug delivery and chemo-photothermal therapy. *Chem Mater* 2017; **29**: 1370-76.
 57. Wang X, Zhang J, Wang Y, Wang C, Xiao J, Zhang Q, et al. Multi-responsive photothermal-chemotherapy with drug-loaded melanin-like nanoparticles for synergetic tumor ablation. *Biomaterials* 2016; **81**: 114-24.
 58. Szakacs G, Paterson JK, Ludwig JA, Booth-Genthe C, Gottesman MM. Targeting multidrug resistance in cancer. *Nat Rev Drug Discov* 2006; **5**: 219-34.
 59. Yu P, Yu H, Guo C, Cui Z, Chen X, Yin Q, et al. Reversal of doxorubicin resistance in breast cancer by mitochondria-targeted pH-responsive micelles. *Acta Biomater* 2015; **14**: 115-24.
 60. Hao T, Chen D, Liu K, Qi Y, Tian Y, Sun P, et al. Micelles of d-alpha-tocopheryl polyethylene glycol 2000 succinate (TPGS 2K) for doxorubicin delivery with reversal of multidrug resistance. *ACS Appl Mater Interfaces* 2015; **7**: 18064-75.
 61. Xing Y, Zhang J, Chen F, Liu J, Cai K. Mesoporous polydopamine nanoparticles with co-delivery function for overcoming multidrug resistance via synergistic chemo-photothermal therapy. *Nanoscale* 2017; **9**: 8781-90.
 62. Wu X, Zhou L, Su Y, Dong CM. A polypeptide micelle template method to prepare polydopamine composite nanoparticles for synergistic photothermal-chemotherapy. *Polym Chem* 2016; **7**: 5552-62.
 63. Zhang R, Su S, Hu K, Shao L, Deng X, Sheng W, et al. Smart micelle@polydopamine core-shell nanoparticles for highly effective chemo-photothermal combination therapy. *Nanoscale* 2015; **7**: 19722-31.
 64. GhavamiNejad A, SamariKhalaj M, Aguilar LE, Park CH, Kim CS. pH/NIR light-controlled multidrug release via a mussel-inspired nanocomposite hydrogel for chemo-photothermal cancer

- therapy. *Sci Rep-UK* 2016; **6**: 33594.
65. Li Z, Hu Y, Jiang T, Howard KA, Li Y, Fan X, et al. Human-serum-albumin-coated prussian blue nanoparticles as pH-/thermotriggered drug-delivery vehicles for cancer thermochemotherapy. *Part Part Syst Charact* 2016; **33**: 53-62.
 66. Zhang X, Nan X, Shi W, Sun Y, Su H, He Y, et al. Polydopamine-functionalized nanographene oxide: a versatile nanocarrier for chemotherapy and photothermal therapy. *Nanotechnology* 2017; **28**: 295102.
 67. Shao L, Zhang R, Lu J, Zhao C, Deng X, Wu Y. Mesoporous silica coated polydopamine functionalized reduced graphene oxide for synergistic targeted chemo-photothermal therapy. *ACS Appl Mater Interfaces* 2017; **9**: 1226-36.
 68. Xue P, Sun L, Li Q, Zhang L, Guo J, Xu Z, et al. PEGylated polydopamine-coated magnetic nanoparticles for combined targeted chemotherapy and photothermal ablation of tumour cells. *Colloid Surface B* 2017; **160**: 11-21.
 69. Wang F, Sun Q, Feng B, Xu Z, Zhang J, Xu J, et al. Polydopamine-functionalized graphene oxide loaded with gold nanostars and doxorubicin for combined photothermal and chemotherapy of metastatic breast cancer. *Adv Healthcare Mater* 2016; **5**: 2227-36.
 70. Lee H, Lee K, Kim IK, Park TG. Fluorescent gold nanoprobe sensitive to intracellular reactive oxygen species. *Adv Funct Mater* 2009; **19**: 1884-90.
 71. Li W, Wang J, Ren J, Qu X. Near-infrared- and pH-responsive system for reversible cell adhesion using graphene/gold nanorods functionalized with i-Motif DNA. *Angew Chem Int Ed* 2013; **52**: 6726-30.
 72. Ding Y, Su S, Zhang R, Shao L, Zhang Y, Wang B, et al. Precision combination therapy for triple negative breast cancer via biomimetic polydopamine polymer core-shell nanostructures. *Biomaterials* 2017; **113**: 243-52.
 73. Liopo A, Su R, Oraevsky AA. Melanin nanoparticles as a novel contrast agent for photoacoustic tomography. *Photoacoustics* 2015; **3**: 35-43.
 74. Repenko T, Fokong S, De laporte L, Go D, Kiessling F, Lammers T, et al. Water-soluble dopamine-based polymers for photoacoustic imaging. *Chem Commun* 2015; **51**: 6084-87.
 75. Ju KY, Kang J, Pyo J, Lim J, Chang JH, Lee JK. pH-Induced aggregated melanin nanoparticles for photoacoustic signal amplification. *Nanoscale* 2016; **8**: 14448-56.
 76. Bayer CL, Nam SY, Chen YS, Emelianov SY. Photoacoustic signal amplification through plasmonic nanoparticle aggregation. *J Biomed Opt* 2013; **18**: 16001.
 77. Gujrati V, Prakash J, Malekzadeh-Najafabadi J, Stiel A, Klemm U, Mettenleiter G, et al. Bioengineered bacterial vesicles as biological nano-heaters for photoacoustic imaging. *Nat Commun* 2019; **10**: 1114.
 78. O'Connor JPB, Jackson A, Parker GJM, Jayson GC. DCE-MRI biomarkers in the clinical evaluation of antiangiogenic and vascular disrupting agents. *Brit J Cancer* 2007; **96**: 189-95.
 79. Longo DL, Arena F, Consolino L, Minazzi P, Geninatti-Crich S, Giovenzana, GB, et al. Gd-AAZTA-MADEC, an improved blood pool agent for DCE-MRI studies on mice on 1 T scanners. *Biomaterials* 2016; **75**: 47-57.
 80. Weissleder R. Molecular imaging in cancer. *Science* 2006; **312**: 1168-71.
 81. Cai WW, Wang LJ, Li SJ, Zhang XP, Li TT, Wang YH, et al. Effective tracking of bone mesenchymal stem cells in vivo by magnetic resonance imaging using melanin-based gadolinium(3+) nanoparticles. *J Biomed Mater Res A* 2017; **105**: 131-37.

82. Xu L, Hong SH, Sun Y, Sun Z, Shou K, Cheng K, et al. Dual T-1 and T-2 weighted magnetic resonance imaging based on Gd³⁺ loaded bioinspired melanin dots. *Nanomedicine: NBM* 2018; **14**: 1743-52.
83. Xu W, Sun J, Li L, Peng X, Zhang R, Wang B. Melanin-manganese nanoparticles with ultrahigh efficient clearance in vivo for tumor-targeting T-1 magnetic resonance imaging contrast agent. *Biomater Sci-UK* 2017; **6**: 207-15.
84. James M, Gambhir S. A molecular imaging primer: modalities, imaging agents, and applications. *Physiol Rev* 2012; **92**: 897-965.
85. O'Connor J, Aboagye E, Adams J, Aerts H, Barrington S, Beer A, et al. Imaging biomarker roadmap for cancer studies. *Nat Rev Clin Oncol* 2017; **14**: 169-86.
86. Ametamey SM, Honer M, Schubiger PA. Molecular imaging with PET. *Chem Rev* 2008; **108**: 1501-16.
87. Frisoni G, Boccardi M, Barkhof F, Blennow K, Cappa S, Chiotis K, et al. Strategic roadmap for an early diagnosis of Alzheimer's disease based on biomarkers. *Lancet Neurol* 2017; **16**: 661-76.
88. Saraste A, Nekolla SG, Schwaiger M. Cardiovascular molecular imaging: an overview. *Cardiovasc Res* 2009; **83**: 643-52.
89. Seagle BLL, Rezai KA, Kobori Y, Gasyna EM, Rezaei KA, Norris JR. Melanin photoprotection in the human retinal pigment epithelium and its correlation with light-induced cell apoptosis. *Proc. Natl. Acad. Sci. U. S. A.* 2005; **102**: 8978-83.
90. Yang M, Fan Q, Zhang R, Cheng K, Yan J, Pan D, et al. Dragon fruit-like biocage as an iron trapping nanoplatform for high efficiency targeted cancer multimodality imaging. *Biomaterials* 2015; **69**: 30-37.
91. Yan F, Zhang Y, Yuan HK, Gregas MK, Vo-Dinh, T. Apoferritin protein cages: a novel drug nanocarrier for photodynamic therapy. *Chem Commun* 2008; 4579-81.
92. Ji T, Zhao Y, Wang J, Zheng X, Tian Y, Zhao Y, et al. Tumor fibroblast specific activation of a hybrid ferritin nanocage-based optical probe for tumor microenvironment imaging. *Small* 2013; **9**: 2427-31.
93. Lin X, Xie J, Zhu L, Lee S, Niu G, Ma Y, et al. Hybrid ferritin nanoparticles as activatable probes for tumor imaging. *Angew Chem Int Ed* 2011; **50**: 1569-72.
94. Hong SH, Sun Y, Tang C, Cheng K, Zhang R., Fan Q, et al. Chelator-free and biocompatible melanin nanoplatform with facile loading gadolinium and copper-64 for bioimaging. *Bioconjugate Chem* 2017; **28**: 1925-30.
95. Ha SW, Cho HS, Yoon YI, Jang MS, Hong KS, Hui E, et al. Ions doped melanin nanoparticle as a multiple imaging agent. *J Nanobiotechnol* 2017; **15**: 73.
96. Xiao W, Li Y, Hu C, Huang Y, He Q, Gao H. Melanin-originated carbonaceous dots for triple negative breast cancer diagnosis by fluorescence and photoacoustic dual-mode imaging. *J Colloid Interf Sci* 2017; **497**: 226-32.
97. Fang RH, Jiang Y, Fang JC, Zhang L. Cell membrane-derived nanomaterials for biomedical applications. *Biomaterials* 2017; **128**: 69-83.
98. Piao JG, Wang L, Gao F, You YZ, Xiong Y, Yang L. Erythrocyte membrane is an alternative coating to polyethylene glycol for prolonging the circulation lifetime of gold nanocages for photothermal therapy. *ACS Nano* 2014; **8**: 10414-25.
99. Jiang Q, Luo Z, Men Y, Yang P, Peng H, Guo R, et al. Red blood cell membrane-camouflaged melanin nanoparticles for enhanced photothermal therapy. *Biomaterials* 2017; **143**: 29-45.
100. Liu F, He X, Zhang J, Chen H, Zhang H, Wang Z. Controllable synthesis of polydopamine

- nanoparticles in microemulsions with pH-activatable properties for cancer detection and treatment. *J Mater Chem B* 2015; **3**: 6731-39.
101. Stritzker J, Kirscher L, Scadeng M, Deliolanis NC, Morscher S, Symvoulidis P, et al. Vaccinia virus-mediated melanin production allows MR and optoacoustic deep tissue imaging and laser-induced thermotherapy of cancer. *Proc. Natl. Acad. Sci. U. S. A.* 2013; **110**: 3316-20.
102. Pedersen JV, Karapanagiotou EM, Biondo A, Tunariu N, Puglisi M, Denholm KA, et al. A phase I clinical trial of a genetically modified and imageable oncolytic vaccinia virus GL-ONC1 with clinical green fluorescent protein (GFP) imaging. *J Clin Oncol* 2011; **29**: suppl.2577.
103. Enochs WS, Petherick P, Bogdanova A, Mohr U, Weissleder R. Paramagnetic metal scavenging by melanin: MR imaging. *Radiology* 1997; **204**:417–23.
104. Kim J, Kim J, Jeong, C, Kim WJ. Synergistic nanomedicine by combined gene and photothermal therapy. *Adv Drug Deliver Rev* 2016; **98**: 99-112.
105. Fan B, Yang X, Li XY, Lv SX, Zhang HH, Sun JH, et al. Photoacoustic-imaging-guided therapy of functionalized melanin nanoparticles: combination of photothermal ablation and gene therapy against laryngeal squamous cell carcinoma. *Nanoscale* 2019; **11**: 6285-96.
106. Karatas OF, Yuceturk B, Suer I, Yilmaz M, Cansiz H, Solak M, et al. Role of miR-145 in human laryngeal squamous cell carcinoma. *Head Neck-J Sci Spec* 2016; **38**: 260-66.
107. Ding Y, Wu Y, Gao W, Zhang C, Zhao Q, Guo H, et al. Analysis of gene expression profiling variations induced by hsa-miR-145-5p-overexpression in laryngeal squamous cell carcinoma cell line Tu-177. *Mol Med Rep* 2017; **16**: 5863-70.
108. Wang J, Guo Y, Hu J, Li W, Kang Y, Cao Y, et al. Development of multifunctional polydopamine nanoparticles as a theranostic nanoplatform against cancer cells. *Langmuir* 2018; **34**: 9516-24.
109. Bhattarai P, Dai ZF. Cyanine based nanoprobess for cancer theranostics. *Adv Healthcare Mater* 2017; **6**: 1700262.
110. Sheng J, Wang XY, Yan JJ, Pan DH, Yang RL, Wang LZ, et al. Theranostic radioiodine-labelled melanin nanoparticles inspired by clinical brachytherapy seeds. *J Mater Chem B* 2018; **6**: 8163-69.